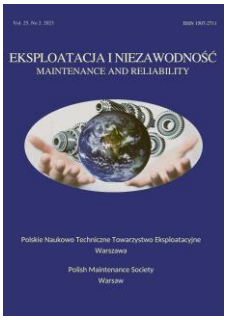

Eksploatacja i Niezawodnosc – Maintenance and Reliability

Volume 28 (2026), Issue 4

journal homepage: http://www.ein.org.pl

Article citation info:
Peruń G, Jurczak W, Kubit A, Trzepeciński T, Przyborski M, Operational diagnostics of propulsion system in modern vessels, Eksploatacja i Niezawodnosc – Maintenance and Reliability 2026: 28(4) http://doi.org/10.17531/ein/221928

Operational diagnostics of propulsion system in modern vessels

Indexed by:
Web of Science Group

Grzegorz Peruń[a], Wojciech Jurczak[b,*], Andrzej Kubit[c], Tomasz Trzepeciński[c], Marek Przyborski[d]

[a] Department of Road Transport, Faculty of Transport and Aviation Engineering, Silesian University of Technology, Poland
[b] Faculty of Mechanical and Electrical Engineering, Polish Naval Academy, Poland
[c] Faculty of Mechanical Engineering and Aeronautics, Rzeszow University of Technology, Poland
[d] Faculty of Navigation and Naval Weapons, Polish Naval Academy, Poland

Highlights

- This study presents operational diagnostics of a VSP across the full load range.
- Vibroacoustic analysis of the structure's accelerations and vibration speeds was proposed.
- Analyses confirm that the change in vibration levels with increasing load is not monotonic.
- The results for the propeller under study were compared with the requirements in standards.
- This study presents operational diagnostics of a VSP across the full load range.

Abstract

This article presents an analysis of vibration measurements of a ship's Voith Schneider Propeller (VSP) system across the full range of the propulsion engine's load. Determining the vibration parameters serves as a form of operational diagnostics for the structural components of this modern propulsion system. This form of diagnostics, based on the analysis of vibration accelerations in three directions relative to the ship's axis as a carrier of information about potential malfunctions and damage, has not yet been given much attention in the literature. The limited number of descriptions and the lack of established vibration signatures for specific VSP malfunctions prompted an examination of the capabilities and benefits of using vibroacoustic methods to analyze the technical condition of a modern vessel's propulsion system. As part of the research, vibration signals were measured and recorded during sea trials on two propulsion units simultaneously across all possible load ranges. Analysis of selected parameters revealed that the propulsion system under examination experiences load levels that, for the propellers in question, should be kept as brief as possible due to their destructive effects, manifested by exceeding permissible acceleration values. The recorded and processed acceleration signals in three directions X (L), Y (H) and Z (V) provide a picture of the exceedances of the permissible operating levels described in standards and the manufacturer's documentation. Particular attention should be paid to the vibration velocity level in the measurement axis, the Z-direction (V), which shows the greatest variation compared to the other measurement directions. In this measurement direction, at a minimum propeller speed of 32 rpm, play in the drive system can be detected (presence of amplitude peaks), and at a maximum propeller speed of 99 rpm, the technical condition of the propeller can be assessed.

Keywords
ship propellers, diagnostics, operation, vibrations

(*) Corresponding author.
E-mail addresses: w.jurczak@amw.gdynia.pl

G. Peruń (ORCID: 0000-0003-1549-0383) grzegorz.perun@polsl.pl, W. Jurczak (ORCID: 0000-0002-1608-7249) w.jurczak@amw.gdynia.pl, A. Kubit (ORCID: 0000-0002-6179-5359) akubit@prz.edu.pl, T. Trzepeciński (ORCID: 0000-0002-4366-0135) ttrzepecinski@prz.edu.pl, M. Przyborski (ORCID: 0000-0001-5354-1407) m.przyborski@amw.gdynia.pl

1. Introduction

Voith marine propellers, also known as VSP propellers, are a specialized type of propulsion system used in marine and river vessels. It is an efficient propeller, invented by Ernst Leo Schneider in 1927. It is a complex design in which the performance of the propeller depends on several parameters [1].

VSPs consist of a vertical shaft with propeller blades. The spindle is mounted inside a cylindrical housing that allows it to rotate around its own axis. Each blade is angled, which allows for the generation of thrust in any direction and ensures very high maneuverability. Thanks to their ability to rotate 360° and generate thrust in any direction, VSPs are particularly useful for maneuvering vessels that require precise control and high maneuverability, such as large vessels, including cargo ships, ferries, tugs, and cruise ships, as well as naval vessels [2]. This propulsion system enables the vessel to move sideways, rotate in place (rotation around its own axis), and control both speed and direction of movement.

The Voith Schneider Propeller (VSP) consists of the following components:

- rotor disk – a circular plate rotating around a vertical axis that serves as the base for the blades,
- vertical blades – arranged around the circumference of the disk, rotating around their own axis and performing a combined rotational and oscillatory motion,
- angle of attack control mechanism (kinematics) – a lever/gear system (known from German as a "koppelgetriebe") used to change the angle of the blades during rotation, responsible for the direction and magnitude of thrust,
- vertical shaft – transmits torque from the motor and drives the rotor casing,
- control point (eccentric), a key element of thrust regulation, whose displacement changes the operating characteristics of the VSP,
- propeller well - a cylindrical structure in the hull that transfers loads to the vessel's structure.

A schematic representation of the GII-type ship-mounted VSP, based on cross-sectional and axial views, is shown in Figure 1a. Figure 1b, on the other hand, shows the appearance of the propeller installed on a vessel. Visible are vertical blades protruding from beneath the hull without a conventional rudder, as the propeller serves as both a propeller and a rudder simultaneously. The axis of rotation is perpendicular to the direction of thrust, and this is a key design difference between the VSP and a typical ship propeller.

a)

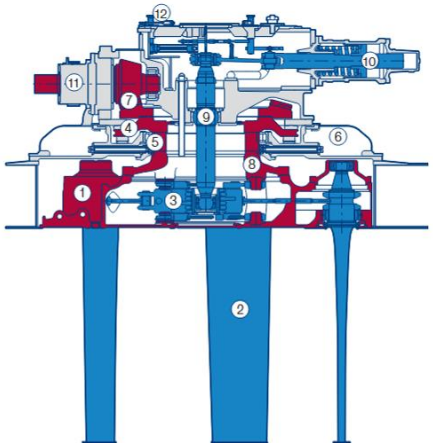

b)

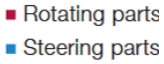

Figure 1. Schematic structure of a GII-type marine VSP, based on a cross-sectional view, an axial view (a), and an actual view of the propeller (b); 1 – rotor casing, 2 – blade, 3 – kinematics, 4 – thrust plate, 5 – roller bearing, 6 – propeller housing, 7 – bevel gear, 8 – driving sleeve, 9 – control rod, 10 – servomotor, 11 – gear pump, 12 – control shaft [2].

The Voith Schneider Propeller differs from a conventional ship propeller drive in that each blade simultaneously performs a rotational movement around the rotor axis and a periodic rotation around its own axis, and during one rotation of the disc, each blade completes one full oscillation cycle. Additionally, there is a phase shift between the blades, and the "suction side" and "pressure side" of the blade alternate during rotation. This results in significantly greater load variability than in a conventional propeller, and translates into: variable hydrodynamic forces, variable torques on the blade control mechanism, bearing loads, and fluctuations in drive torque [3]. In practice, this means that the VSP is not a source of a single

"simple" blade-passing-frequency excitation known from conventional propellers, but rather a multi-harmonic excitation strongly dependent on the blade pitch kinematics, eccentricity, the vessel's motion state, and flow inhomogeneities. More recent unsteady models show that the coupled motion of the blades induces nonlinear, transient changes in hydrodynamic forces, and thus also a more complex spectrum of excitations transmitted to the propeller foundation and to the stern areas [4,5].

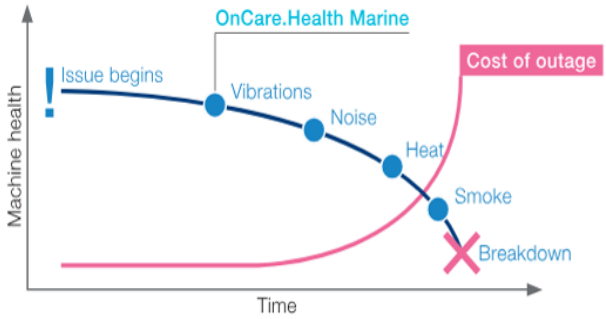

Figure 2. A simplified illustration of the successive stages of operation, along with the associated signs of changes in technical condition and maintenance costs, according to the propulsion system manufacturer [2].

Early detection of operational issues is the foundation for safe, long-term operation and cost savings. Diagnostics, not limited to propeller vibrations, is a key element recommended by the manufacturer, as shown in Fig. 2. Fig. 3, in turn, shows the layout and types of factory-installed sensors, taken from the propeller documentation, used to control and protect the propeller's components.

Figure 3. Components of VSP diagnostics [2].

2. Problem formulation and literature review

The impact of vibrations throughout the ship's structure generated by VSP propulsion systems is poorly documented in the literature, while vibrations in the propulsion system itself remain the subject of ongoing research, due to the unique nature of its operation. A review of the literature indicates that three main sources of excitation causing ship structure vibrations from VSPs are most commonly identified [2,4,6].

The first source is mechanical excitation: forces and moments transmitted through the propeller shaft, bearings, pitch control mechanism, and drive foundation. An analysis of the vibrations of a cycloidal propeller blade during maneuvers alone shows that strong load fluctuations generate not only a risk of blade fatigue but also load variability in the prime mover and the entire support structure.

The second source consists of hydrodynamic forces acting on the hull and stern, caused by the unsteady pressure field and the pulsating flow behind the VSP. Reference [6] describes studies on the vibration response of the stern of a ship equipped with a straight-bladed/cycloidal propeller. This publication presents separate modeling of forces due to bearing forces and forces due to surface forces acting on the hull structure. The authors demonstrate that both components are significant for predicting stern vibrations. The second source involves hydrodynamic excitations on the hull and stern, caused by a non-stationary pressure field and a pulsating flow behind the VSP.

The third source, which is also the focus of the current research, involves cavitation and flow separation from the blades, which generate pressure pulses and amplify both local vibrations and underwater noise. Publication [7] demonstrates that under high VSP loads, cavitation occurs primarily within a limited range of blade angles; sheet cavitation and intermittent tip vortex cavitation were primarily observed, and the cavitation effect can influence the blade design, amplifying the unsteadiness of the phenomenon.

The best source of knowledge regarding the origin of vibrations is research in the fields of blade dynamics and unsteady hydrodynamics. In [3], it was shown that during states such as bollard pull, crash stop, crabbing, turning, or zig-zag, VSP blades experience highly variable periodic loads. This is significant because for VSP-propelled vessels and ferries, it is

precisely these maneuvering states that are often critical for operational performance, not just straight-line travel. Such conditions also occur at maximum speed, as demonstrated in the research section of this article. Recent publications [8,9] confirm that the coupled motion of VSP blades induces nonlinear changes in hydrodynamic forces; therefore, from the perspective of hull vibrations, complex transient excitation should be expected, not just a single dominant frequency [8,9]. Vibration measurements can be performed using non-contact methods with gravimeters, laser displacement sensors, and vibration velocity sensors, as demonstrated in the diagnostic literature [10,11,12]. In contrast, thrust force measurements can be performed using a strain gauge array that measures axial compression of the shaft. This is a key parameter determining the actual thrust force, which simultaneously loads the bearings. The authors used this measurement technique in the cited specialist literature [13,14].

This article narrows the scope of diagnostic measurement to the vibrations of VSP propulsion systems, with the aim of preventing damage or malfunctions in the propulsion system components themselves. This research area is niche, as the literature directly describing the diagnosis of VSP damage through vibration analysis is very limited. Available studies focus mainly on: variable blade loads and their fatigue effects, loads and the susceptibility of the propulsion and steering system, the influence of cavitation and ventilation on dynamic forces, and the consequences for bearings, gearboxes, and the blade pitch mechanism. This means that a significant portion of diagnostic conclusions must be derived indirectly, based on damage mechanics and load models, rather than on numerous operational fault-diagnosis studies for VSPs.

Vibration measurements for VSPs are particularly important because they identify damage at the very early stages of deterioration. The propeller manufacturer emphasized this in its documentation, as shown earlier in Figure 2. In the VSP design, each blade completes a full cycle of pitch change during a single rotor revolution, resulting in highly periodic and time-varying loads on the blade, blade hub, bearings, and pitch control system. It was explicitly stated that, compared to a conventional propeller, such conditions cause higher load fluctuations, which in turn leads to fatigue loads on the blades and to changes in the main drive load. In models of this type, components related to the hydrodynamic torque on the blade shaft, friction torques in the blade bearings, and friction torques in the rotating assembly bearings are also explicitly present. From the perspective of damage, this means that vibrations are not only a symptom of the propeller's operation but also a mechanism accelerating degradation. In the literature on VSP blade dynamics, the vibration problem is primarily associated with fatigue risk, and in studies on multi-link and multi-body models with the load on the control and motion transmission system [9]. A proposed structure for a diagnostic system that integrates the diagnostic process with the causes of damage and the prediction of technical condition - i.e., production and operational diagnostics - is presented in [14].

The VSP design described above shows that a typical system consists of: blades, blade shafts/pins, blade bearings, rotor bearings, a thrust plate, a gearbox, a drive sleeve, a control rod, a servo mechanism, and a pump. The description of the design also indicates that the blade shafts are supported by slide bearings or special rolling bearings, protected by seals, while the rotor is supported axially by a thrust plate and radially by a roller bearing. On this basis, five main classes of damage/malfunctions can be identified for which vibrations are a significant symptom or mechanism of degradation: 1) blades and their roots, 2) blade bearings and rotor bearings, 3) blade control system: control rods, levers, joints, servo drive, 4) the gearbox and torque transmission path, 5) seals and components exposed to secondary effects of leakage or increased resistance to movement [2]. This conclusion is partly a direct result of the VSP's design and partly inferential - but it is well-founded from a mechanical standpoint.

The most extensively documented topic in the literature on VSPs concerns the issue of blade fatigue damage. Reference [3] shows that, due to the specific kinematics of VSPs, the blades are exposed to high load fluctuations, which directly translates into fatigue loading on the blade. The authors analyze blade vibrations under various maneuvering conditions, such as bollard pull, crash stop, crabbing, turning, and zig-zag - that is, precisely the operating regimes in which VSP-equipped tugs and ferries are used. From a diagnostic standpoint, this means that an increase in the amplitude of vibrations associated with periodic blade loading should be treated as a potential indicator of: fatigue fracture, a decrease in blade stiffness, play in the

mounting, or degradation of the blade–shaft connection. The literature itself does not yet provide a comprehensive catalog of damage spectra for VSPs, but it shows that the hydrodynamic–structural coupling is sufficiently strong for changes in the blade's structural properties to affect thrust, torque, and dynamic response [9]. Additionally, in publication [9], the authors, writing about fluid–structure interaction, demonstrated that structural deflections of the blade interact with the hydrodynamic load and affect thrust and torque. This is important in the context of damage, because even moderate degradation of stiffness or the initiation of a crack can not only increase vibrations but also alter hydrodynamic loads, thereby creating a self-amplifying mechanism.

The most natural area for vibration diagnostics of the drives under analysis is the blade and rotor bearings. VSP blade dynamic models explicitly account for bearing friction torque on both the blade shaft and the disc/rotor assembly. This is very important because it indicates that the condition of the bearings is not merely an operational detail, but a component of the equations of motion and the forces acting within the system. In operational practice, it is reasonable to assert that wear, increased friction, misalignment, or play in blade bearings or rotor bearings should manifest as changes in the vibration spectrum and drive torque. Direct publications such as "fault signature of VSP blade bearing spall" are practically nonexistent, but the theoretical literature provides a strong basis for treating bearings as a critical element for vibration diagnostics.

The design of the VSP confirms that the blade bearings and the main rotor bearings transmit both geometrically forced loads and forces resulting from thrust and tilting forces. From a failure perspective, it should therefore be concluded that symptoms such as an increase in blade-motion-related harmonics, an increase in broadband vibration energy, and an increase in resistance torque are the most likely indicators of bearing failure. This passage is partly the result of inference, but it is directly supported by the fact that the model literature explicitly introduces bearing friction as a dynamic parameter.

From an operational standpoint, the literature highlights leaks and the ingress of seawater into the propeller's internal channels. The VSP design description indicates the presence of seals that protect the bearings from oil leaks and water ingress. The manufacturer has also published service information regarding the main sealing rings, warning that incorrect configuration of the spacer elements can lead to serious leakage. This is not vibration literature in the strict sense, but it is worth considering in a review of potential VSP failures, as leakage can secondarily lead to deteriorated lubrication conditions, increased friction, bearing degradation, and consequently to increased vibration levels [15]. This latter relationship is a mechanically obvious inference, but the issue of leakage and its criticality is directly confirmed by the source.

According to the manufacturer's documentation [2], Voith propellers utilize condition monitoring systems that track critical drive components and are designed to alert operators to anomalies in order to prevent more serious damage. This confirms that, in practical operation, the issue of VSP condition diagnostics is a real and evolving concern. At the same time, there are very few publications in the open scientific literature that provide ready-made vibration signatures for specific VSP faults, e.g., separately for blade bearing wear, setting joint misalignment, bevel gear damage, or blade fracture. The state of knowledge is therefore asymmetrical: the sources of dynamic loads have been well identified, but mapping these loads to specific classes of diagnostic faults is significantly less developed. Limiting ourselves solely to damage/malfunctions of propulsion system components, the following problem groups are most extensively documented in the technical literature [2]: fatigue of blades and blade roots - directly confirmed by blade vibration analyses and high load fluctuations [9], degradation of blade bearings and rotor bearings – strongly supported by dynamic models in which bearing friction torques are an explicit component of the loads, as well as by the very architecture of VSPs, malfunction of the blade pitch mechanism – well supported by FEM studies and investigations into the influence of the control mechanism on blade motion, loads, and the dynamic behavior of the drive [16], damage to gearboxes and power transmission components – particularly in connection with ventilation, for which there are direct indications of reported damage to bevel gears and other mechanical parts [7,15], and secondary degradation from cavitation/ventilation – not so much due to classical erosion as to impulsive and transient overloads.

The impact of science on the development of machine

diagnostics, with a particular focus on maritime applications, is discussed in the article [17]. The article concisely summarizes the achievements of the past 50 years, illustrating how approaches have evolved alongside advances in computer processing power and the development of measurement equipment. The authors discuss how these changes can contribute to improving the process of diagnosing vessel propulsion systems.

The problem of vibration diagnostics in ship propulsion systems, specifically, the assessment of mechanical energy transferred from the main engine to the ship's propeller, which is dissipated as a result of propeller shaft vibrations - has been described in the paper [18]. The author states that estimating the amount of energy generated by a propeller shaft subjected to transverse vibrations allows for an assessment of the performance of a ship's propulsion system during energy transfer and its conversion into work and heat.

To effectively improve the efficiency of the VSP drive, the paper [19] utilized the periodic characteristics of the coupled motions of the VSP drive to transform the complex spatial motion of the blades into a parameterized analysis of two-dimensional plane curves. The presented method, based on controlling the parameters of the motion curve, is of some significance for optimizing the efficiency of the VSP drive.

The work [20] presents experimental modal studies of the VSP drive. In order to reduce the influence of vibration stresses generated by the cycloidal drive, and in particular the sing phenomenon, as well as to reduce the influence of critical vibration speeds and to avoid resonance between the frequencies of the ship's hull and equipment and the propeller frequencies and the torque frequency, deconvolution was applied.

The blade-strut interface of a VSP experiences high stress concentrations due to geometric features such as fillets, keyways, and thread reliefs. In the study [21] a global model of the VSP was developed and static sub-modeling in Ansys Mechanical was used to analyze stress concentrations at this joint location. In the authors' opinion conventional global finite element analysis often misses these local stresses, leading to unexpected component failures.

The transfer matrix model of the propulsion shafting system, established to describe the dynamic behavior is presented in turn [22]. In the model the dynamic characteristics of oil film within thrust bearing are considered.

The article [23] discusses the results of propeller load calculations obtained using commonly applied methods implemented by the authors in propeller shaft calculation software. Practical recommendations are presented for determining the hydrodynamic loads on the propeller in the absence of the data necessary to perform full calculations. The procedure for verifying the propeller load with respect to shaft alignment criteria is discussed.

The article [24] analyzes the motion of a VSP-type cycloidal propeller characterized by unstable vibrations and derives an analytical expression for the maximum angular acceleration of the blade rotation at a given angular velocity and eccentricity. Based on this, two sets of cycloidal propellers with opposite rotation directions were constructed, and CFD simulation was used to reproduce operating conditions in a two-dimensional plane, where the mechanism generates different directions and magnitudes of thrust for autonomous propulsion from a stationary state, and the dynamic parameters of the propellers were obtained based on the motion state of the mechanism.

To summarize the above literature review of existing research, in light of the available sources, vibrations in VSPs, considered solely in terms of damage or malfunction of propulsion system components, should be interpreted primarily as a problem of blade fatigue, bearing degradation, malfunction of the pitch mechanism, and gearbox overloads caused by unsteady hydrodynamic forces, cavitation, and ventilation. The best-documented issues are: blade fatigue and dynamic overloads of the mechanism and drivetrain; the least developed area remains the open literature on diagnostic signatures of specific VSP faults based on vibrations.

3. Research scope and assumptions

The purpose of vibration diagnostics is to identify the causes of high vibration amplitudes. It is also important to determine the period during which the machine can be safely operated. Corrective actions - that is, identifying the scope of work and spare parts needed to eliminate the hazard - are also crucial. It is therefore also important to conduct a detailed analysis of the vibration signals. During the analysis, it should be remembered that the most common causes of increased vibration include:

imbalance in rotating masses, misalignment between the drive shaft and the driven shaft, shaft deflection, and bearing play or damage.

All machines and equipment, including propulsion systems, emit vibrations, and this is a normal phenomenon caused by their operation. Vibration measurements are performed to analyze any irregularities that occur. Analyses are conducted in accordance with the recommendations of EN ISO 20816 [25], and in the case of ships - Defense Standard NO-20-A500-3 regarding "Technical Requirements and Testing of Ship Equipment and Mechanisms – Vibrations - Measurements and Evaluation Criteria" [26].

In the process of determining the overall assessment of a cycloidal drive, a key role is played by determining the root mean square (RMS) values of accelerations or vibration velocities characterizing the vibration process. By determining the RMS value of vibrations in relation to the limit values for a given group of machines, the dynamic condition of the equipment can be assessed. In practice, four classification zones are distinguished: A, B, C, and D. These are assigned equipment conditions defined as good, satisfactory, temporarily acceptable, and unacceptable.

The subject of the research described in this article were Voith-manufactured Schneider (Turbo) 21GH/160 propellers in service on the vessel. The propulsion system of the vessel under study consists of two shaft lines between the main engines and the cycloidal propellers, each with flexible couplings, a gearbox, and a bulkhead seal. The Voith propeller on the port side of the ship, on which the measurements were taken, is a propeller characterized by a relatively low number of operating hours. Due to its shortest operating time on the vessel, it served as the basis for comparisons in the diagnostics of the second propeller. The characteristics of the left- and right-side cycloidal propellers of the 21GH/160 type, manufactured by the German company Voith Turbo, are presented in Table 1.

During operation of a VSP propulsion system - a type of marine propulsion system that uses an azimuth propeller - the propulsion system's structure may undergo certain deformations. These deformations are influenced by various factors mentioned earlier, such as dynamic loads, temperature, and load cycles. The Voith propeller under examination may be subjected to load cycles, including changes in load and direction of rotation. These cycles can cause fatigue in the structural materials and lead to microcracks, deformations, and potential damage. The best way to minimize deformation on a Voith drive is to follow proper maintenance, operation, and usage practices, including recommendations that can help manage deformation: regular inspections and maintenance, monitoring operating parameters, vibration control, proper loading and avoidance of excessive loads, high-quality materials and construction, etc.

Table 1. Specifications of the Voith Turbo 21GH/160 cycloidal propeller [2].

Parameter	Value	Unit
Maximum propeller shaft speed when operating on main engines	611	rpm
Maximum propeller shaft speed when operating on electric motors	229	rpm
Maximum propeller speed during operation on main engines	101	rpm
Maximum propeller speed during operation on electric motors	37	rpm
Nominal power	970	kW
Number of blades	5	-
Blade rotation diameter	2100	mm
Blade length	1600	mm
Weight	15400	kg
Weight with oil	17200	kg

The vibrations generated by a Voith propeller during operation can cause structural deformation or damage to the propeller components. It is particularly important to monitor and minimize these vibrations in order to avoid adverse effects such as material fatigue or bearing damage.

The attempt described in this article to determine the technical condition of a ship's propellers using vibroacoustic diagnostics is a response to the above requirements. The research involved conducting a series of measurements of the vibration accelerations of the port and starboard propellers of the vessel under test, across the full range of propeller loads. This propeller load was increased incrementally during the measurements and covered its entire possible range, from 32 to 99 rpm.

4. Experiment preparation

Measurements were taken on the structures of both propellers, primarily using vibration accelerometers. The accelerometers were mounted on the Voith propeller housing, and they were used to measure vibration accelerations in three mutually perpendicular directions designated X (L), Y (H), and Z (V), where X is the horizontal longitudinal direction (also designated as L), along the ship's axis; Y is the horizontal (H) transverse direction, perpendicular to the ship's axis in the horizontal plane; and Z is the direction perpendicular to both X and Y in the vertical (V) plane.

The signal waveforms were recorded using a 16-channel RogaDAQ16 data acquisition card and DasyLab software. IMI604B ICP triaxial vibration accelerometers were used for the measurements, and the sampling frequency of the recorded signals was fs = 11,025 Hz. The sensors used complied with the requirements of ISO 20816-1 [25], and their most important parameters are presented in Table 2.

The propellers are were mounted to the hull structure using special flexible rings that dampen vibrations and reduce their amplitude. For this reason, the measurement points where vibration acceleration waveforms were recorded during tests of the port and starboard propellers, designated as M-1, were located near the propeller blade control mechanism (Fig. 4). In these areas of the propeller structure, accelerations can be recorded for the most significant sources of Voith propeller vibration [3] affecting the assessment of the operational condition of the gearbox bearings.

Table 2. Characteristics of the IMI 604B triaxial vibration accelerometers [27].

Performance	English	SI
Sensitivity (± 20 %)	100 mV/g	10,2 mV/(m/s^2)
Measurement range	± 50g	± 490 m/s^2
Frequency range (± 3 dB)	30 ÷ 300 000 cpm	0.5 ÷ 5000 Hz
Resonant frequency	600 kcpm	10 kHz
Broadband resolution (1÷10 000 Hz)	350 µg	3,434 µm/sec^2

a) b)

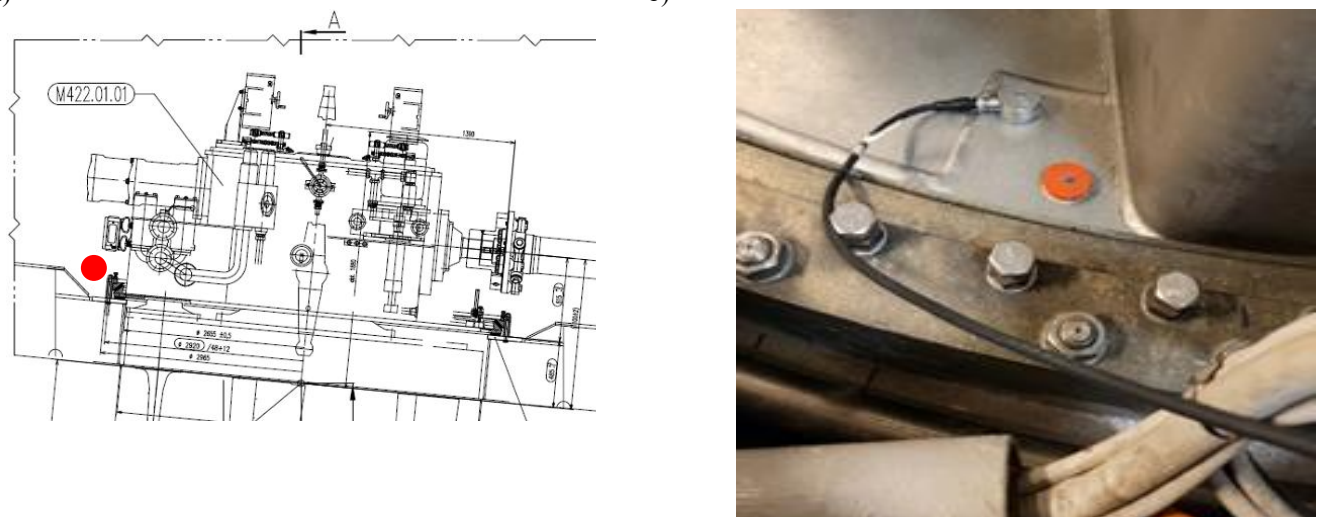

Figure 4. Location of the measurement point: a) schematic, b) actual - installation of the accelerometer on the portside propeller structure of the ship.

For selected areas of the monitored portside propeller structure, a steel accelerometer housing was attached directly (i.e., without any spacers) to the austenitic steel substrate. The method of mounting the accelerometer on the starboard-side propeller was identical to that used on the port side (see Figure 5).

Due to weather conditions, measurements of the propeller located on the port and starboard sides were conducted on several occasions. The analyzed measurement results were obtained under similar hydrometeorological conditions.

During vibration recording, the recorded results were monitored online using DasyLab software communicating with the data acquisition card, in order to perform a preliminary verification of measurement accuracy. However, the actual analyses were performed only after the measurement cycle was completed in the Matlab computational environment. For this purpose, an application was developed for direct conversion of measurement data from the DasyLab format to the native

Matlab format, as well as custom algorithms that expanded the capabilities of the analyses and significantly accelerated and automated the processes. The initial stage of the analysis was the conversion of values, taking into account the calibration data of the sensors used.

The sensitivity of each channel with respect to each of the IMI sensors used was:

- **604B91/SN29301**/ICP in the direction:
  X (L) - 99mV/g (10,1mV/m/s^2), Y (H) - 98mV/g (10mV/m/s^2), Z (V) - 89mV/g (9,1mV/m/s^2),
- **604B91/SN29271**/ICP in the direction:
  X (L) - 96mV/g (9,9mV/m/s^2), Y (H) - 96mV/g (9,8mV/m/s^2), Z (V) - 95mV/g (9,7mV/m/s^2).

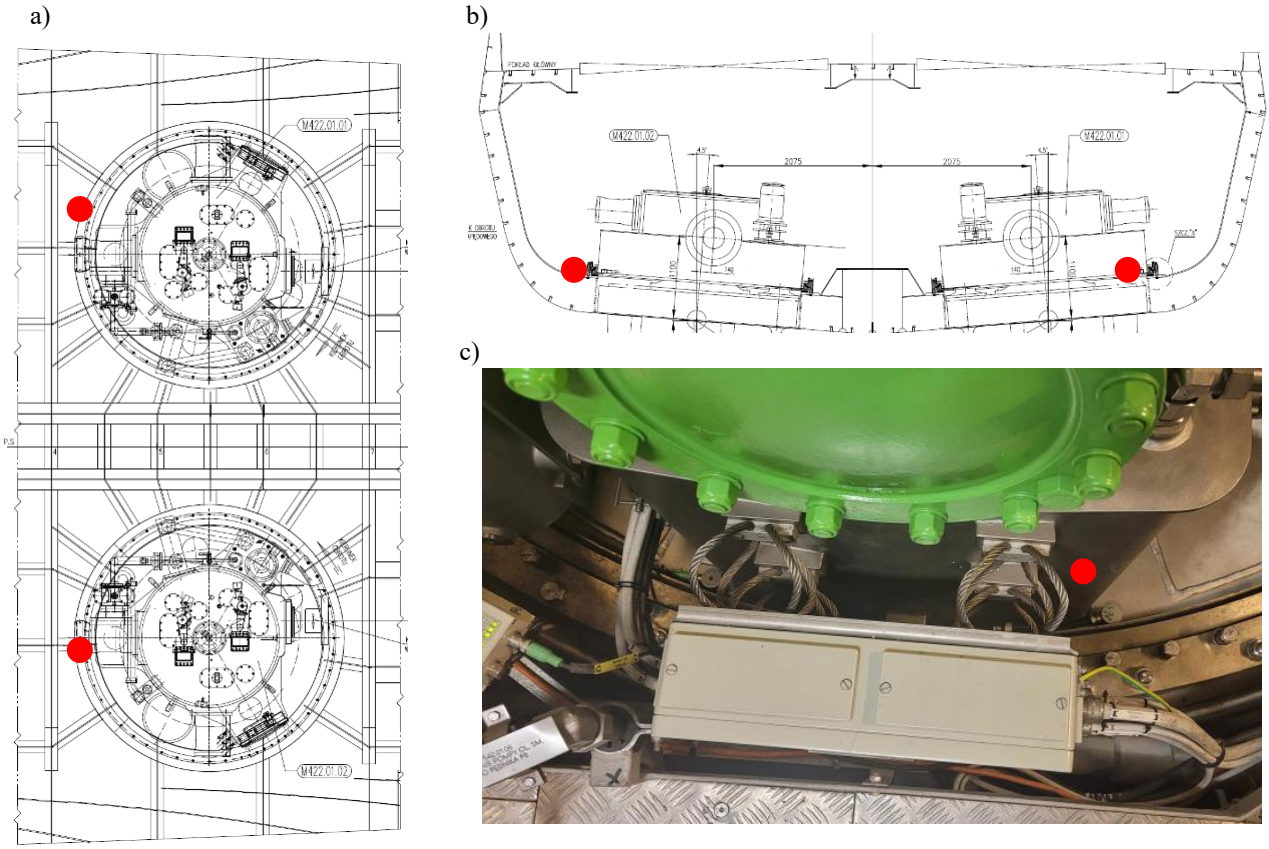

Figure 5. Layout of the propulsion room showing the area (marked with ●) where the accelerometers were mounted: a) bottom view, b) cross-section [2], c) location of the accelerometer on the starboard propeller based on the propeller housing.

5. Experiment and result analysis

Vibroacoustic signals can be analyzed in various ways, ranging from simple time-domain analyses - using, among other methods, statistical analysis - to the determination of frequency spectra, as well as more advanced analyses, such as time-frequency analyses [28]. The scope of the analysis results presented in this article is consistent with the overarching objective of the research, which was to determine the operational suitability of propellers in accordance with the PN-ISO 18616 standard and to compare vibration levels with the permissible level specified in NO 20-A500-3. For this reason, it was necessary to determine the vibration velocity waveforms, which were achieved by numerically integrating the recorded acceleration waveforms. Both the recorded acceleration waveforms and the calculated vibration velocity waveforms were analyzed in strictly defined intervals, for which it was conventionally assumed that they were determined for specific, constant operational parameters of the propulsion units, i.e., the assumed combinations of speed and loads of the ship's propulsion system. The full-load range of the propulsion system has been divided into (approximately) two-minute intervals, as shown in Fig. 6.

The main part of the analysis was performed using Matlab software and a proprietary library of signal processing algorithms. The root mean square (RMS) value was adopted as the primary measurable and comparable parameter in the studies. As previously noted, although measurements were

conducted continuously during the ship's mission, the analyses were performed on segments of the recorded signals extracted from the entire data set. An example of a vibration acceleration signal, recorded in the X (L) direction and obtained during one of the measurement cycles, divided into successive load stages, is shown in Figure 6 to illustrate the adopted method of analysis.

Table 3 shows the relationship between the rotational speed of the VSP propellers and the rotational speed of the drive motor for the full measurement range, broken down into the assumed load intervals labeled 1 through 8.

The gear ratio in the VSP mechanism is fixed, but this does not guarantee constant absolute speeds. For a typical Voith VSP shaft line, a turbo-coupling or hydrodynamic coupling is used in the drive train, and the hydrodynamic coupling exhibits load-dependent slippage.

The ship's port and starboard VSP operate in opposite directions to counteract transverse forces but should be a "mirror image" of each other's parameters; however, on the vessel under examination, the port-side propeller was replaced due to a malfunction. Furthermore, the fixed gear ratio applies only to each individual shaft line, and if a hydrokinetic clutch is present, slippage under load may cause differences in the recorded rotational speed (rpm) of the shaft and the propeller, which can also be observed in the Table 3.

The test results are presented below, grouped by type of parameter analyzed. Analyses of acceleration and vibration velocity are presented separately for each section, with results shown for the port and starboard propellers.

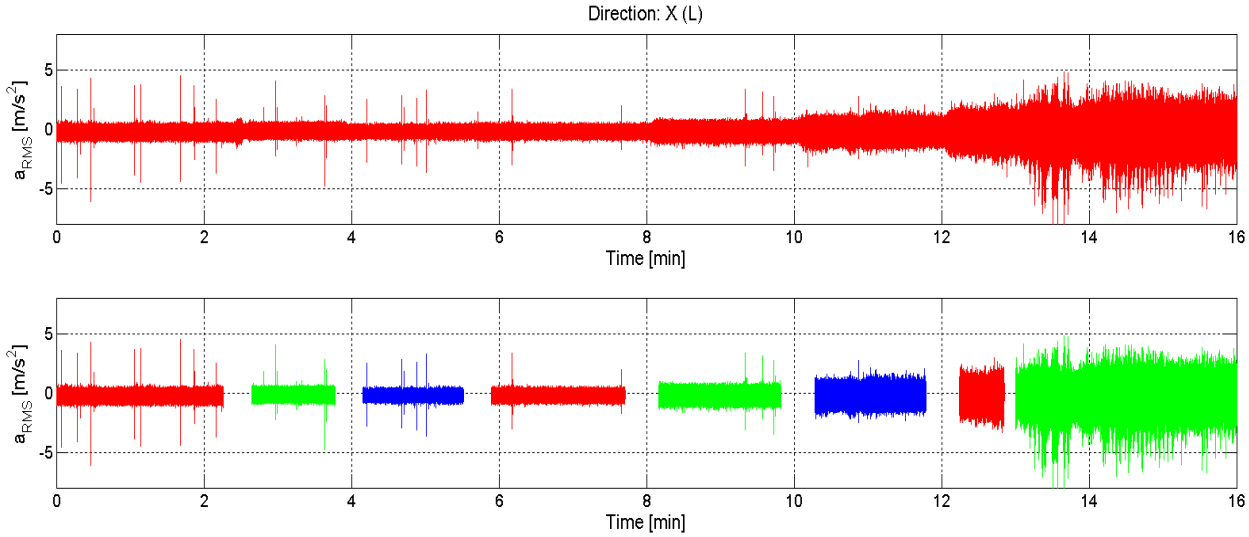

Figure 6. Time course of vibration accelerations recorded on the ship's port propeller for the selected X (L) direction, divided into propeller load stages.

Table 3. Relationship between the rotational speed of VSP propellers and the rotational speed of the drive motor.

Analysis interval number	**Engine rotational speed** [rpm]	**Propeller rotational speed** [rpm]	**Analysis interval number**	**Engine rotational speed** [rpm]	**Propeller rotational speed** [rpm]
1	600	32	5	1400	75
2	800	42	6	1600	91
3	1000	53	7	1800	96
4	1200	64	8	1900	99

5.1. Methodology of signal processing

Vibroacoustic phenomena occurring during equipment operation can be used as a source of information about its technical condition, but determining this condition often requires different signal processing methods. The approach to analysis depends on the object and subject of the study, the type of signal being analyzed, the method and location of its acquisition, and many other factors. By monitoring vibration levels and/or measuring accompanying noise, it becomes possible to predict and prevent failures caused, for example, by excessive wear or developing damage. This is a difficult task, as it usually requires a thorough understanding of the phenomena occurring within the equipment under examination. The

presented research should be considered exploratory for the propulsion systems of the analyzed vessel.

There is no single, universally effective algorithm for proceeding, just as there is no single universal measurement location independent of the design and mode of operation of the object under study. When performing analyses, researchers look for certain signal metrics that are sufficiently well correlated with the phenomenon under study. Depending on the situation, a variety of analysis methods may be employed. In the simplest diagnostic cases, it may suffice to determine a single metric whose variations reflect the intensity of the phenomenon under investigation. Typically, however, it is necessary to determine many different metrics and search for correlations between their values and changes in the device's condition.

Among all the time-domain signal analysis methods used in the study, only those that proved to be sensitive to changes in the vessel's operating conditions will be described below, and their results are presented later in the article [29–32]. These also include dimensionless discriminants used in the diagnostics of various components and devices, e.g., rolling bearings, gearboxes, and internal combustion engines. These values were determined based on converted into physical acceleration values, and in the case of velocity signals, after numerically integrating the vibration acceleration waveforms individually in each of the eight analyzed intervals corresponding to successive operating regimes of the propulsion units.

The conversion from the measured voltage signal *U(t)* into vibration acceleration *a(t)* may be written as:

$$a(t) = \frac{U(t)}{S_{sen}} \tag{1}$$

where:

a(t) – vibration acceleration [m/s^2],

U(t) – measured sensor output voltage [mV],

S_{sen} – sensor sensitivity [mV/(m/s^2)],

- Average value $\bar{x}$:

$$\bar{x} = \frac{1}{T}\int_{t_0}^{t_0+T} x(t)\ dt \tag{2}$$

where:

x(t) – analyzed signal (acceleration or vibration velocity),

t, t₀ – time, initial time,

T – averaging time.

- Peak value x_{peak}:

$$x_{peak} = \max_{t_0<t\le t_0+T}(|x(t)|) \tag{3}$$

- Root mean square valuex_{RMS}:

$$x_{RMS} = \sqrt{\frac{1}{T}\int_{t_0}^{t_0+T} x^2(t)\ dt} \tag{4}$$

- Peak-to-peak value x_{P-P}:

$$x_{P-P} = \left|\max_{0<t\le T}\big(x(t)\big) - \min_{0<t\le T}\big(x(t)\big)\right| \tag{5}$$

- Variance$v$:

$$v = \frac{1}{T}\int_{t_0}^{t_0+T}[x(t)-\bar{x}]^2\ dt \tag{6}$$

- Standard deviationσ:

$$\sigma = \sqrt{\frac{1}{T}\int_{t_0}^{t_0+T}[x(t)-\bar{x}]^2\ dt} \tag{7}$$

- Average deviation (mean deviation) MD:

$$MD = \frac{1}{T}\int_{t_0}^{t_0+T}|x(t)-\bar{x}|\ dt \tag{8}$$

- Crest factor C:

$$C = \frac{x_{peak}}{x_{RMS}} \tag{9}$$

- Clearance factor L:

$$L = \frac{x_{peak}}{\left(\frac{1}{T}\int_{t_0}^{t_0+T}\sqrt{|x(t)|}\ dt\right)^2} \tag{10}$$

- Impulse factor I:

$$I = \frac{x_{peak}}{\frac{1}{T}\int_0^T |x(t)|\ dt} \tag{11}$$

5.2. Analysis of vibration acceleration signals – portside propeller

Based on observations of the time courses of vibration acceleration amplitudes recorded in three directions over the course of a single test cycle, measured on the ship's port propeller across the entire propeller load range - i.e., from 600 to 1900 engine rpm (corresponding to 32 to 99 rpm propeller rotational speed), an increase in vibration acceleration amplitude is observed as propeller load increases. The graph for the X (L) direction is shown in Figure 6; a comparison of all other directions is presented in Figure A1 in Appendix 1.

A distinct increase in vibration amplitude is observed when the propeller speed exceeds 75 rpm, which corresponds to an engine speed of 1,400 rpm. Transient impulse disturbances are also visible throughout the entire test period, particularly intense at low propeller loads of approximately 32 rpm. The

amplitudes of these transient disturbances reach values approximately 4–5 times greater than the average amplitude in this measurement range. The area where disturbances occur and their intensity indicate that this load range should be monitored more frequently during ad hoc vibration measurements and evaluated for suitability and service life as described in the standard in categories A through D.

The processed results of the vibration measurements recorded on the portside propeller by sensor with serial number SN29301, grouped by measurement direction - i.e., the X (L), Y (H), and Z (V) directions - are shown in Figure 7.

As can be seen, the root-mean-square values of vibration accelerations in each direction for propeller speeds up to approximately 64 rpm are similar. At higher rotational speeds, the component recorded in the Z direction begins to clearly exceed the components in the X (L) and Y (H) directions. To provide a complete picture of the root-mean-square vibration accelerations, Figure A2 in Appendix 2 also shows the root-mean-square accelerations in the resultant direction.

For the first four analysis intervals, similar root-mean-square values of vibration accelerations were obtained, below 0.4 m/s² for each component and approximately 0.6 m/s² when analyzing the resultant values. At higher rotational speeds, there is a noticeable increase in the analyzed measure, even up to approximately threefold.

The next stage of the analysis involved determining changes in commonly known statistical and diagnostic measures in each of the analyzed ranges. For this purpose, 17 parameters were determined, the most significant of which are presented in the following graphs. Figure 8a refers to the X direction (L), 8b to the Y direction (H), and 8c to the Z (V) direction. The graphs present the relative value of selected measures in the analyzed interval relative to the maximum value of the measure obtained during the tests for a given propeller, in this case the portside propeller. This approach allows one to assess the sensitivity of a given measure to changes in the operational parameters of the vessel under study.

Standard and average deviations, variances vary in a similar manner to the root mean square value - which is taken as the baseline in these studies - regardless of the direction analyzed. Measures such as Crest Factor, Clearance Factor, and Impulse Factor, known from the diagnostic literature [33–36], exhibit a different pattern of variation. The absolute values of these measures can be used in further studies of the unit's drive after its assumed operating life, and the observed differences may be one of the symptoms of wear or emerging malfunctions.

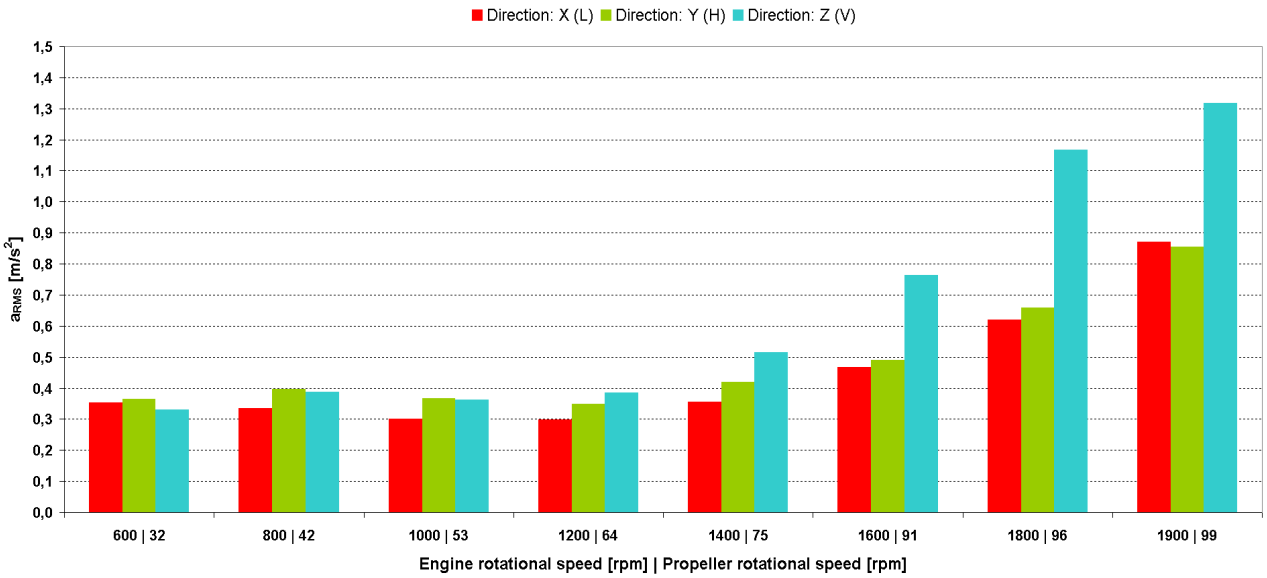

Figure 7. Summary of the root-mean-square vibration accelerations of the port propeller for the entire range of propeller loads as a function of the drive motor's rotational speed in the mutually perpendicular directions X (L), Y (H), and Z (V).

a)

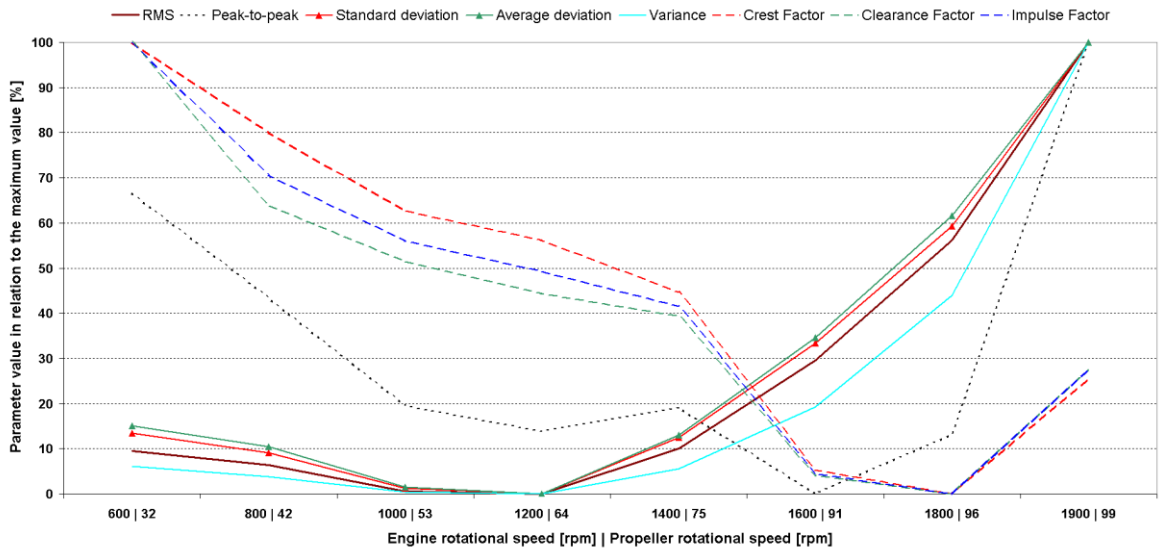

b)

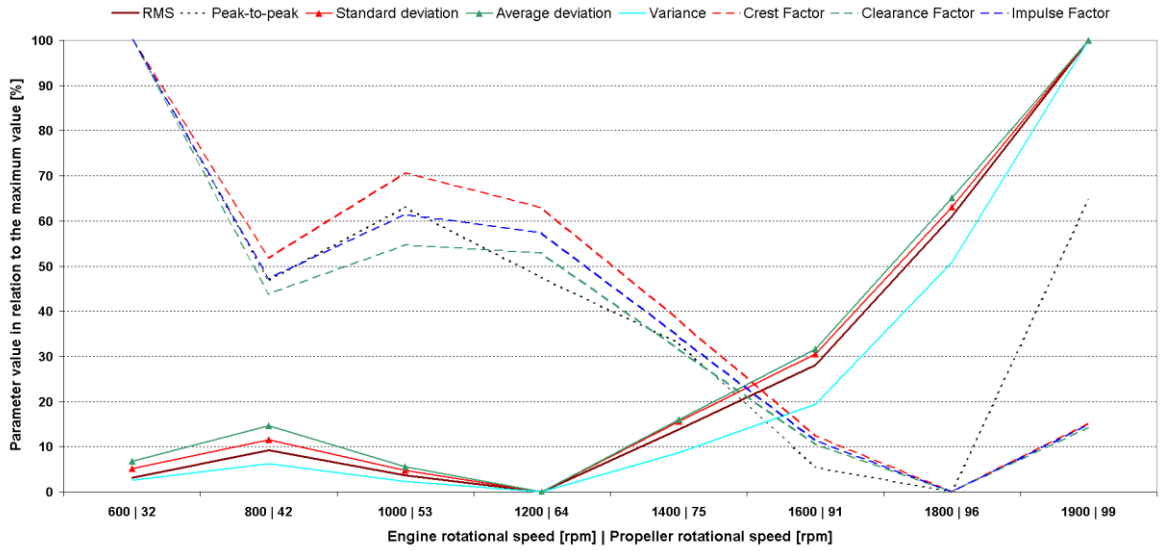

c)

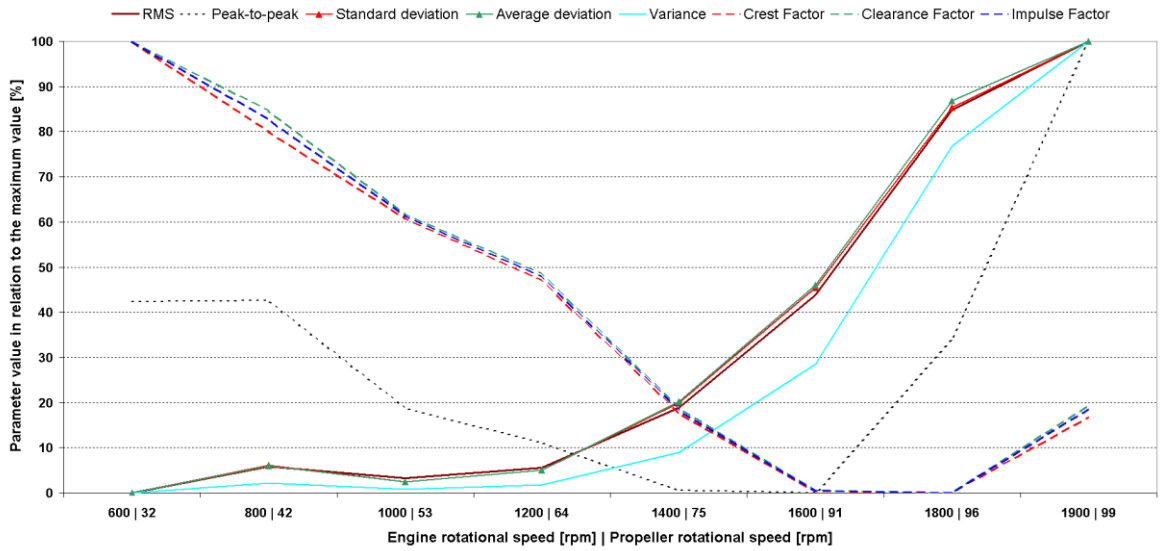

Figure 8. Summary of percentage changes in selected statistical and diagnostic measures for the analyzed load ranges of the port propeller.

5.3. Analysis of vibration acceleration signals – starboard propeller

Similar to the analysis of measurements taken for the port propeller, the recorded vibration acceleration signals from the starboard propeller were processed. The overall time courses of the vibration acceleration amplitudes recorded in three directions during a single full test cycle, measured on the ship's starboard propeller, are presented in Figure A3 in Appendix 3.

As expected and consistent with previous results, an increase in propeller load corresponds to an increase in the amplitude of vibration accelerations recorded at the test measurement point (Fig. 5c). The graphs presented in Fig. A2 show increasing amplitudes of vibration accelerations, especially after the propeller reaches a rotational speed of 75 rpm (1400 engine rpm). Impulse-like disturbances were also recorded across the entire range. This applies to every propeller load range, though these disturbances are significantly less intense than those occurring on the portside propeller (see Fig. A1). Changes in vibration acceleration amplitudes caused by load variations can be used to determine useful, safe, and long-term operating ranges for the propellers under test. They can also serve as a basis for a quick, relatively simple assessment of the propulsion system's technical condition.

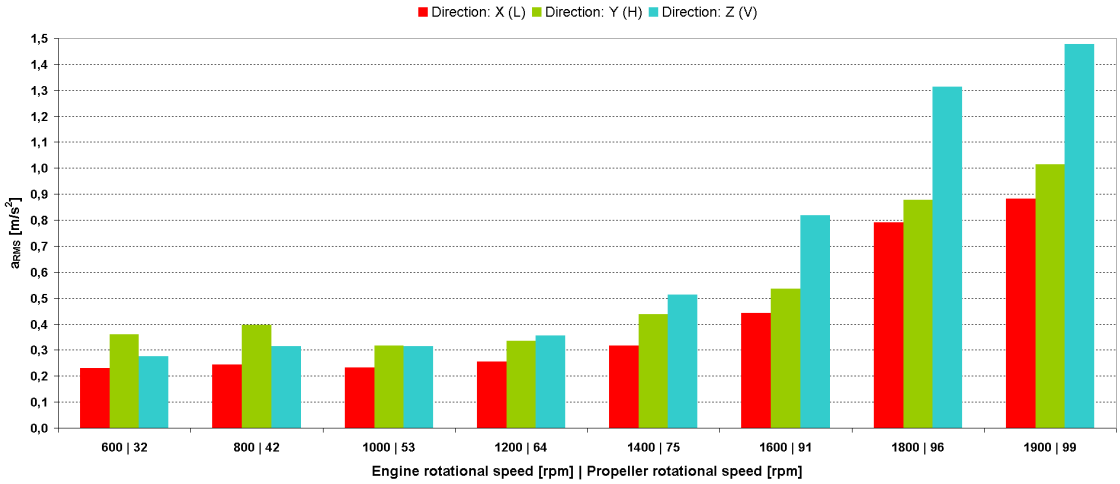

Figure 9. Summary of the root-mean-square vibration accelerations of the starboard propeller for the entire range of propeller loads as a function of the drive motor's rotational speed in the mutually perpendicular directions X (L), Y (H), and Z (V).

As with the portside propeller, the main part of the analysis was conducted on isolated segments of the recorded signals for specific propeller load parameters. The determined effective values of vibration accelerations in each tested speed and load range of the starboard propeller at the analyzed measurement point are presented in Fig. 9, grouped by individual measurement directions: X (L), Y (H), and Z (V). Figure A4 in Appendix 4 also shows the calculated effective values of vibration accelerations in the resultant direction at the tested measurement point.

As with the port propeller, the values in the Z direction are also several dozen percent higher than in the other two directions. The RMS values determined for low loads on the starboard propeller turn out to be slightly lower than those obtained for the port propeller. For the three highest loads, higher values were obtained; however, the RMS of vibration accelerations for both propellers can be considered similar.

The nature of the changes in RMS values in the resultant direction (Fig. A4) is also similar to the corresponding results for the port propeller. For propeller rotational speeds up to approximately 64 rpm, the RMS values are approximately 0.5 m/s², increasing to approximately 2 m/s² in the higher load range, compared to 1.8 m/s² for the port propeller.

Figure 10 presents the results of the next stage of the analysis. The relative values of the selected measures in the examined range were again normalized to the maximum value of the measure obtained during the tests, this time for the starboard propeller.

The results for the Z (V) direction are similar to those obtained for the portside propeller. A different pattern of changes is observed for the X (L) and Y (H) directions. In particular, for the Y (H) direction, the waveforms of all measures selected for presentation show consistency. It is assumed that this is due to a significantly lower number of

impulse disturbances in the recorded signal for the first half of the analyzed intervals, which resulted in an increase in measures such as Crest Factor, Clearance Factor, and Impulse Factor for the port propeller.

a)

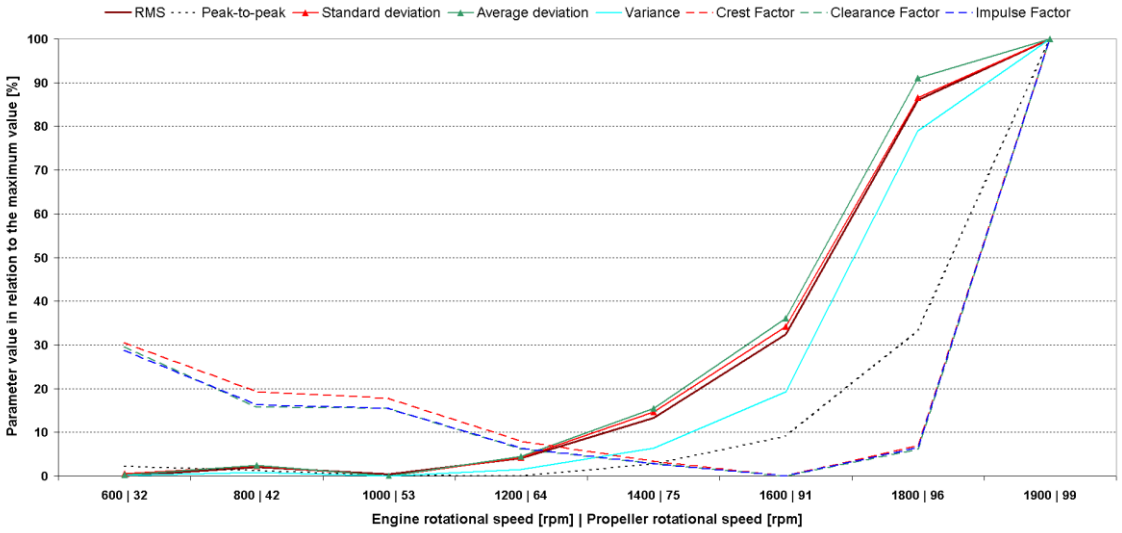

b)

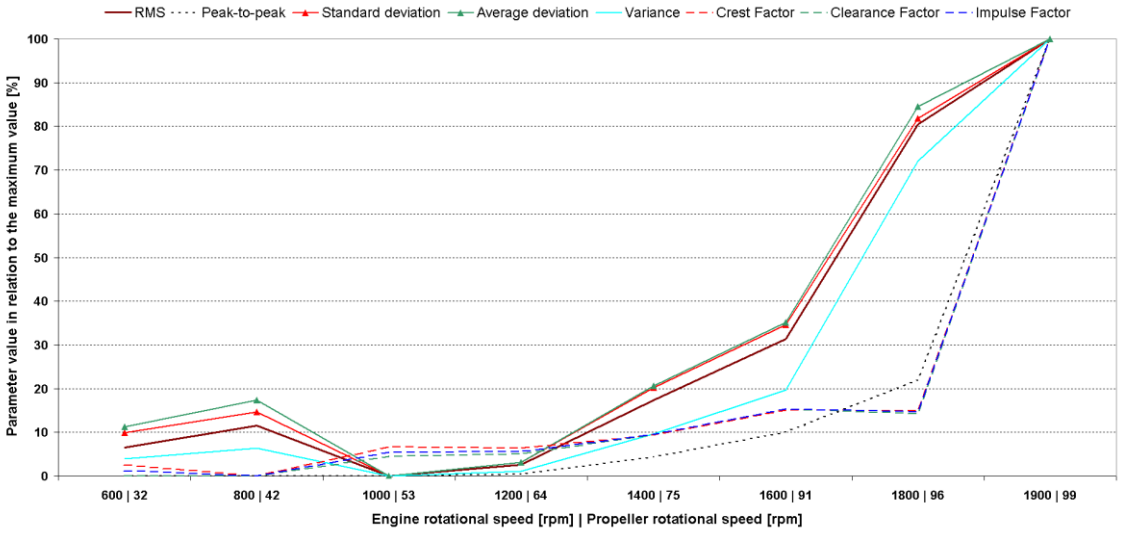

c)

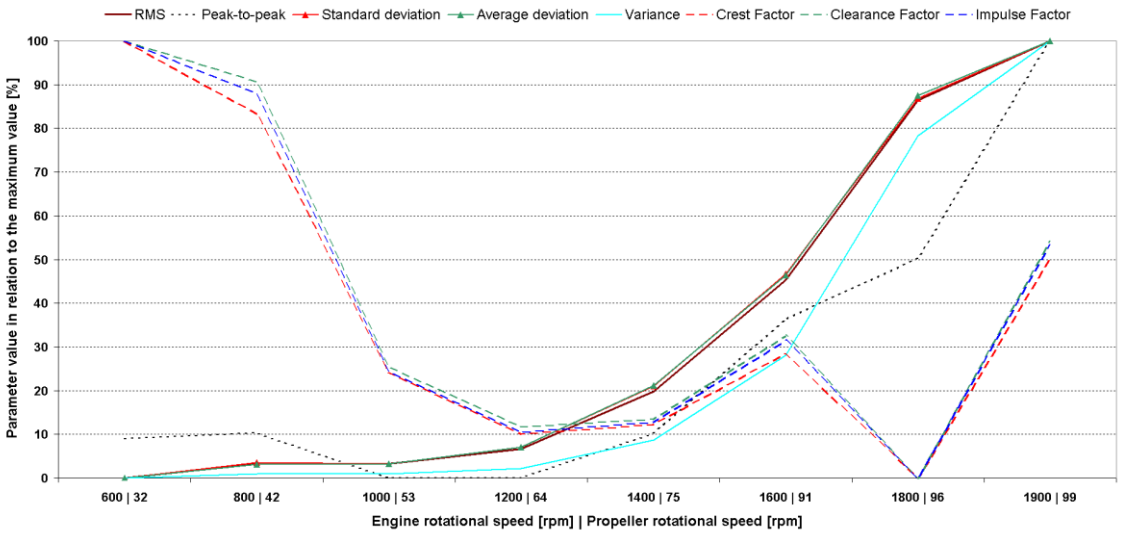

Figure 10. Summary of percentage changes in selected statistical and diagnostic measures for the analyzed load ranges of the starboard propeller.

5.4. Analysis of vibration velocity signals

During the vibration-based diagnostics, the provisions of ISO 20816 must be taken into account; this standard classifies machines into four groups based on their type, as well as their rated power or shaft diameter (Table 4).

Table 4. Typical limit values for vibration velocity amplitude and the corresponding vibration intensity classification zones according to ISO 20816 [25].

V_{RMS} value [m/s] x10^{-3} in the range of 2-1000 [Hz]		Group			
above	up to	I	II	III	IV
	0,71	A	A	A	A
0,71	1,12				
1,12	1,8	B	B	B	B
1,8	2,8				
2,8	4,5	C	C	C	C
4,5	7,1				
7,1	11,2	D	D	D	D
11,2	18				
18					

A – good condition; B – satisfactory condition; C – still acceptable condition; D – unacceptable condition.

Group I includes machines with a rated power exceeding 300 kW. The speed range is between 120 rpm and 15,000 rpm. Sliding bearings are often incorporated into the design of this type of machine. According to the standard, Group II comprises machines with a rated power between 15 kW and 300 kW. Group III includes pumps with multi-vane impellers and a separate drive, with a power rating exceeding 15 kW. The design of such machines very often incorporates either sliding or rolling bearings. The ISO 20816 standard also defines Group IV, which includes pumps with multi-vane impellers and built-in drives. These are centrifugal pumps with mixed flow and axial flow with a power rating above 15 kW.

In accordance with ISO 20816-1, machine assessment zones are established. The vibrations of new machines that have been put into service are classified as Zone A. This thus indicates that the machine is in good condition. The standard also defines Zone B, where machines are capable of operating without restrictions. This is referred to as an acceptable condition. Machines may be deemed unsuitable for long-term operation until appropriate preventive measures are implemented. In such cases, they are classified in Zone C, which is still considered an acceptable condition. In light of the standard's provisions, Zone D is also distinguished. It is this zone that defines the machine's condition as unacceptable. Table 4 also presents the typical limit values for the vibration intensity classification zones according to ISO 20816.

The vibration acceleration waveforms obtained during the tests were integrated in each of the eight analyzed intervals, each characterized by a specific engine/propeller rotational speed and load. Subsequently, like the acceleration waveforms, they were analyzed in the Matlab environment.

Due to the adopted sampling frequency of the vibration acceleration signals, which was 11,025 Hz - resulting from the frequency range of the sensors used in the measurements (see Table 2) - the initial signal processing was performed up to a frequency of 5 kHz. An example of the vibration acceleration spectrum in the Z (V) direction is shown in Figure 11.

Integration of the vibration acceleration waveforms was performed on the recorded signals after low-pass filtering. The filter cutoff frequency was 5 kHz. Figure 12 shows example vibration velocity spectra in the Z direction (V) for the portside (a) and starboard (b) propellers, respectively.

Due to the absence of significant amplitudes in the higher frequency band, the analyzed band was limited to 1 kHz, which is in accordance with the requirements of the standards. Because there are no additional diagnostic components in the band above 500 Hz, the frequency range of the spectrum has been limited to 0–500 Hz to ensure the clarity of the graphs

At an engine speed of 800 rpm, the fundamental frequency is approximately 13.33 Hz, and its fourth harmonic is approximately 53.33 Hz. The clearly visible component of approximately 53.58 Hz in the spectrum (and in the subsequent vibration speed spectra presented in Figure 12) thus indicates the dominance of the fourth harmonic of the engine speed,

which attests to the ordered, deterministic nature of the excitation associated with the operation of the VSP propulsion system and the drive system. In addition, in the lower frequency band, components associated with the fundamental rotational frequency and its lower harmonics are observed, while in the range of approximately 90–120 Hz, additional frequency components with lower amplitudes are present, reflecting the complexity of the system's dynamic response.

The results presented in the following graphs for individual directions and the full range of actuator loads, measured in time intervals of approximately 2 minutes per load, were compiled into tables and compared to the values specified in ISO 20816-1. Subsequently, to determine the condition of the tested drive unit and fulfill the main objective of the presented tests, the results were referenced to standard NO 20-A500-3. The classification of devices into specific machine groups in accordance with NO-20-A500-3:2017 is presented in Table 5 [27].

The rated power of the propulsion units on the vessel under test is 970 [kW], and the rotational speed depends on the type of propulsion (electric motors/main engines). For the main engines tested, the maximum engine rotational speed is 1900 rpm, and the corresponding propeller rotational speed is 99 rpm. For a drive shaft rotational speed exceeding 1400 rpm, corresponding to 75 rpm of the propeller, there is a maximum 100% deflection of the propeller's five blades, and within this range, vibrations are felt on the upper decks. The vessel achieves a cruising speed of 10.6 knots in the aforementioned range, and 14 knots at 99 rpm of the propeller.

The vibration intensity zone, according to the above standards, classifies the propellers under test in Group III. The test object should be classified in Machine Group C, in accordance with NO-20-A500-3:2017.

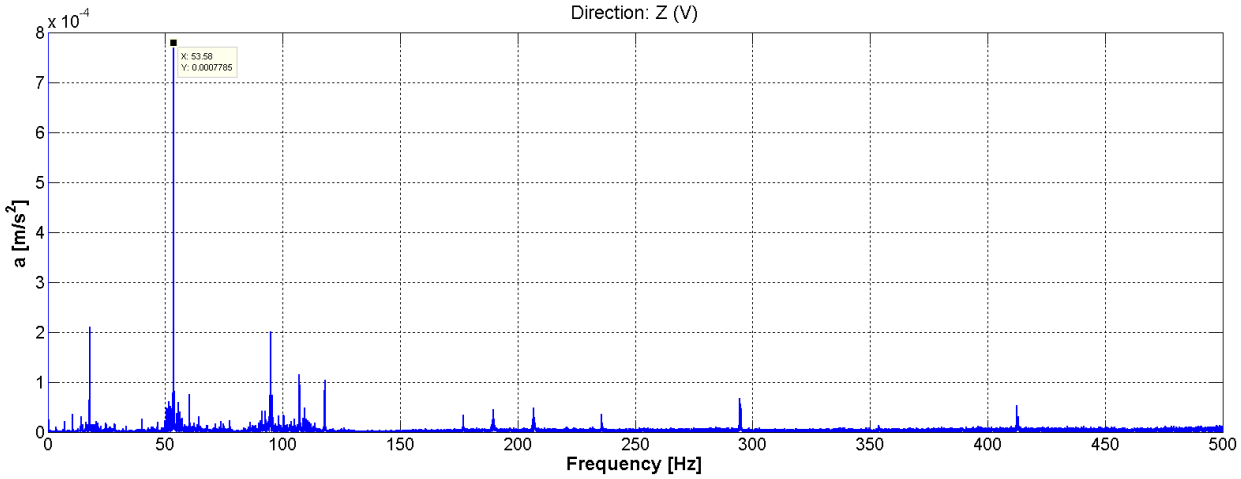

Figure 11. Sample spectrum of vibration accelerations recorded on the port propeller in the Z (V) direction, with an engine speed of 800 rpm.

a)

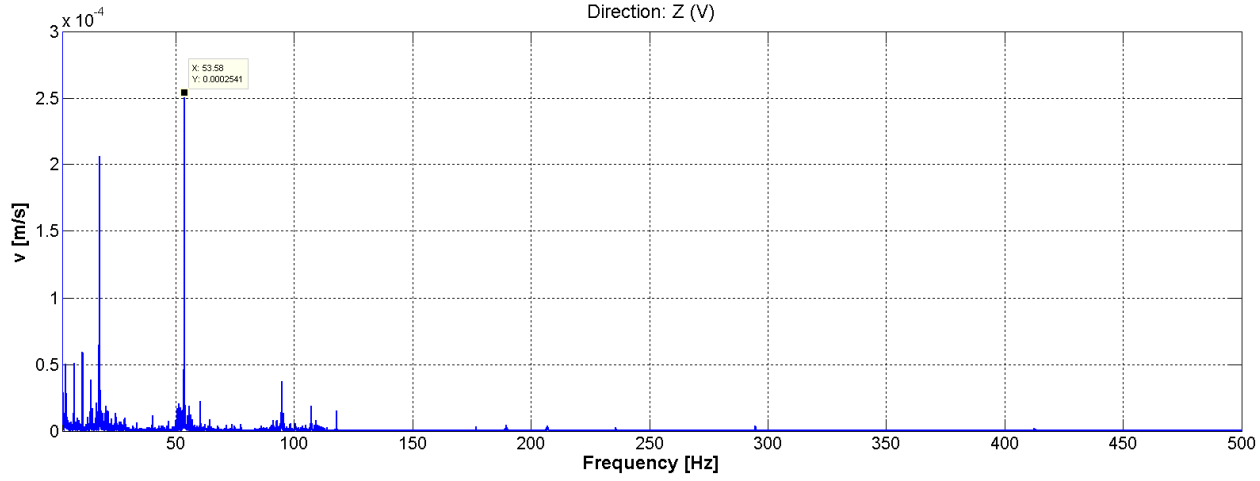

b)

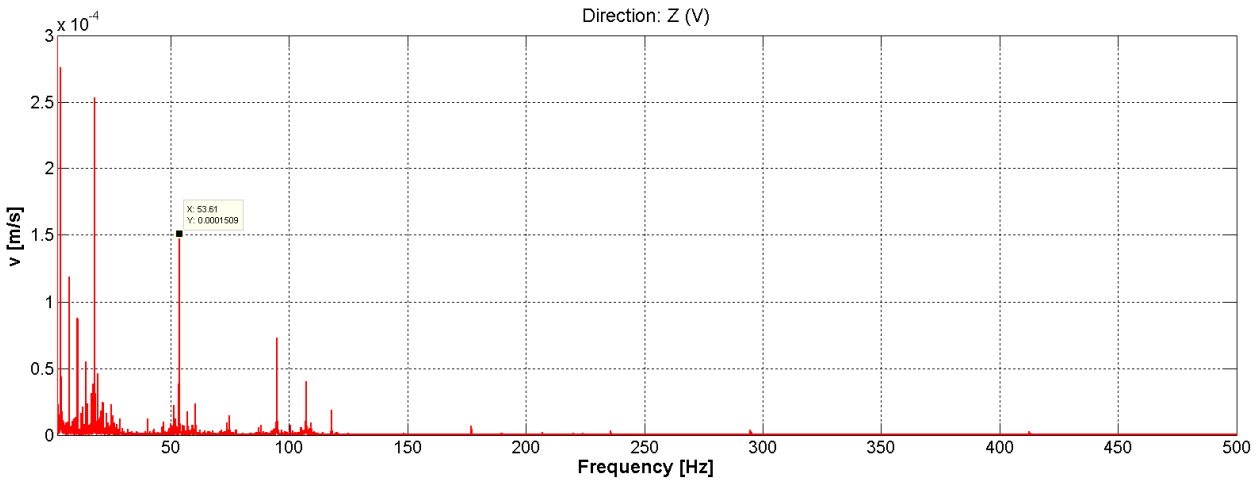

Figure 12. Examples of vibration velocity spectra recorded in the Z direction (V), with an engine speed of 800 rpm: a) on the port propeller, b) on the starboard propeller.

In both spectra, a component at approximately 53.58 Hz is clearly prominent, allowing it to be unambiguously linked to the fourth harmonic of the motor's rotational speed. The dominance of this rotational frequency component indicates that the system's dynamic response in the vertical direction is orderly and is related to the cyclic excitation generated by the operation of the propulsion system and the propeller. This phenomenon is of significant diagnostic importance, as it indicates that the vibration energy is not randomly distributed across a wide frequency band, but is concentrated in specific rotational speed orders. Such a spectral pattern is typical for systems in which kinematic, hydrodynamic, or structural excitations synchronized with rotational motion play a fundamental role.

In the low-frequency part of the spectrum, i.e., below approximately 20 Hz, significant components corresponding to the fundamental rotational frequency and its lowest multiples are also observed. Their presence indicates that, in addition to the dominant fourth harmonic in the dynamic response, there are also excitations associated with the system's fundamental rotational motion, which may be related to load asymmetry, misalignment, eccentricity, local structural compliance, or the manner in which vibrations are transmitted from the drive system to the hull and foundations. From the perspective of this study's objective, it is particularly important that the spectra allow these mechanisms to be distinguished and demonstrate that the vibration response is not limited solely to the first rotational order.

In the range of approximately 90÷120 Hz, additional, less intense components are visible, which can be interpreted as higher harmonics, combination frequencies, or the effect of local amplification of the structural response. Their amplitudes are clearly lower than that of the 53.6 Hz component; however, their presence confirms the complex nature of the dynamic response of the system under study. At the same time, the absence of a significant broadband increase in vibration levels in the higher frequency range suggests that deterministic excitations dominate in the analyzed operating condition, rather than strong random or impulse phenomena.

Table 5. Classification of equipment into specific machine groups in accordance with NO-20-A500-3:2017 [27].

Device group	Device subgroup	Machinery and equipment
A		Internal combustion engines with
	Aa	a piston stroke of:
	Ab	- less than 700 mm,
	Ac	- between 701 and 1,400 mm,
		- 1,401 mm or more.
B		Vertical pumps, centrifugal fans, etc.
		Units with electric motors.
		Propeller shaft and intermediate shaft of the drive system.
C		Horizontal pumps, centrifugal pumps, axial fans, etc.
		Units with electric motors featuring a horizontal drive shaft.
		Turbine combustion engines and their components.
		Gearboxes and bearings for the main drive shaft line.

A comparison of the spectra recorded on the port and starboard propellers indicates that, although the positions of the main frequency components remain similar, their amplitudes

are not identical. This means that both propellers are subject to the same excitation mechanism but differ in their dynamic response conditions. These differences may result from variations in the local structural stiffness, differences in damping, hydrodynamic operating conditions, the technical condition of the components, or the vibration transmission path. From a scientific point of view, this is a valuable observation, as it confirms that spectral analysis can be used not only to identify characteristic frequencies but also to assess the asymmetry in the operation of both drive systems.

5.5. Analysis of vibration velocity signals – portside propeller

The effective vibration velocity values obtained through measurements and numerical integration for specific propeller loads across all load regimes - i.e., 600–1900 rpm, corresponding to 32–99 rpm of the propeller - are shown in Figure 13 for the X (L), Y (H), and Z (V) directions, and in Figure 14 for the resultant direction. A reference to the values specified in ISO 20816-1 is presented in Table 6, in which the resultant direction is denoted by the letter W.

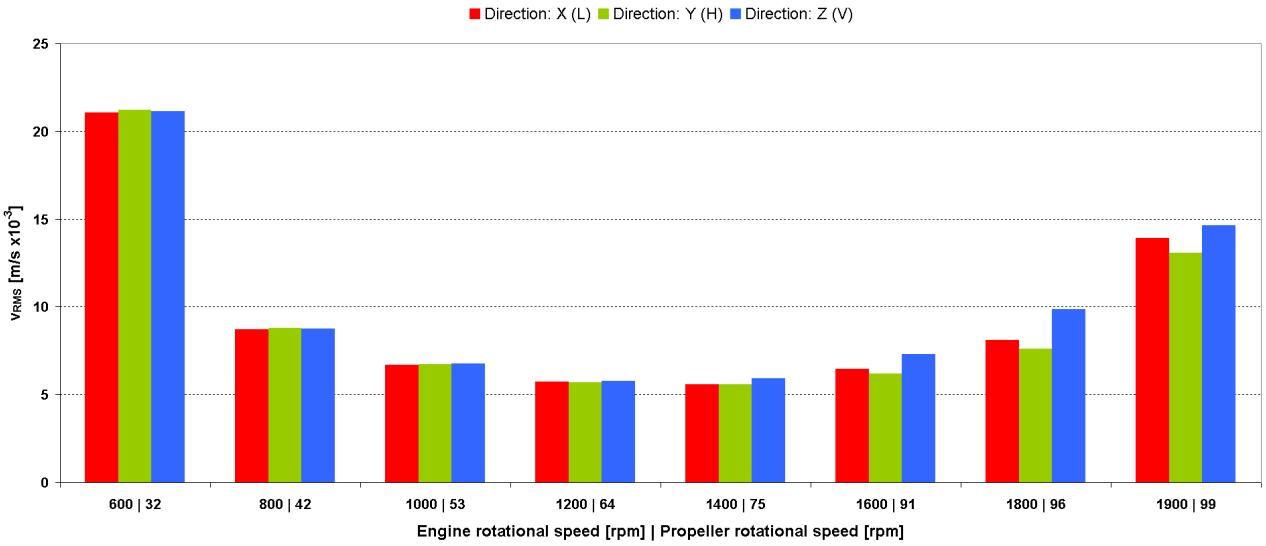

Figure 13. Summary of the root-mean-square values of the port propeller's vibration velocity for the entire range of propeller loads as a function of the drive motor's rotational speed in the mutually perpendicular directions X (L), Y (H), and Z (V).

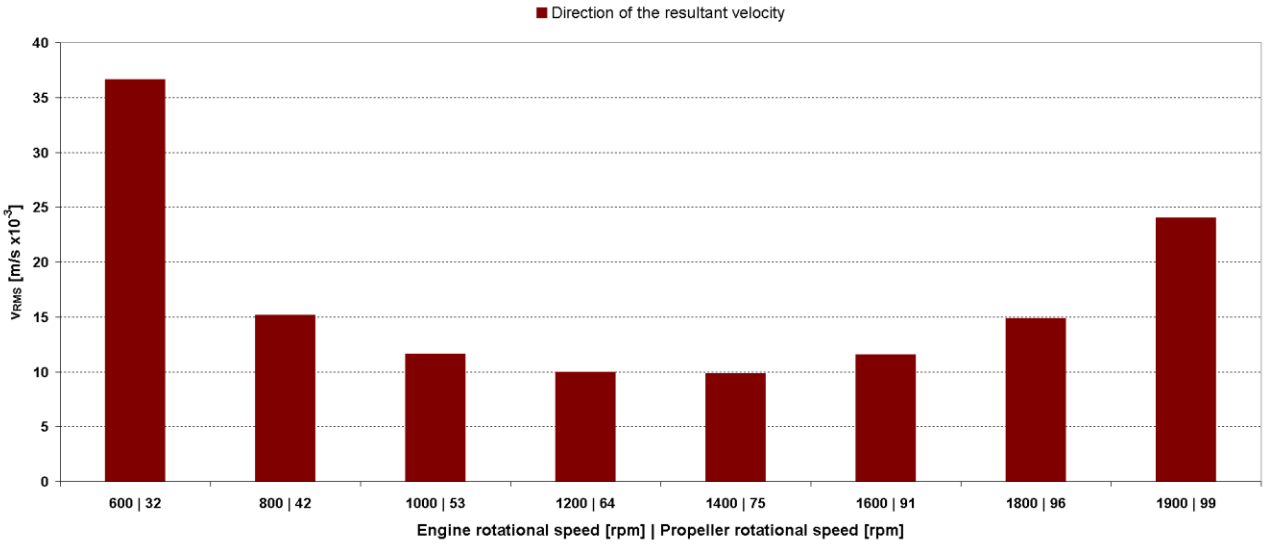

Figure 14. Summary of the root-mean-square vibration velocities in the resultant direction for the portside propeller across the entire range of propeller loads as a function of the drive motor's rotational speed.

The measured vibration velocity values in the X (L) and Y (H) directions are similar across all analyzed ranges, showing the greatest variation - approximately 6–7% for the last two rotational speeds tested. Up to a speed of 1400 rpm, the values

in the Z (V) direction are also very similar. A greater variation in the root-mean-square vibration velocity values in the Z (V) direction relative to the other two directions, amounting to several percent, appears in ranges starting from an engine speed of 1600 rpm. Above 1,500 rpm of the engine, and thus 80 rpm of the propeller at 100% propeller blade deflection, the propeller's vibrations are primarily influenced by vibrations in the Z (H) direction.

Table 6. Effective vibration velocity values for the entire load range of the port propeller.

Engine speed – operating mode	Propeller speed – operating mode	RMS vibration velocity V_{RMS} [mm/s] Direction X (L)	Direction Y (H)	Direction Z (V)	*Direction W**	Vibration intensity zone according to ISO 20816-1 for class III
600	32	21,1	21,2	21,2	36,6	D
800	42	8,7	8,8	8,7	15,1	C
1000	53	6,7	6,7	6,8	11,7	C
1200	64	5,7	5,7	5,8	9,9	C
1400	75	5,6	5,6	5,9	9,9	C
1600	91	6,5	6,2	7,3	11,5	C
1800	96	8,1	7,6	9,9	14,9	C
1900	99	13,9	13,1	14,6	24,0	D

** resultant direction.*

The permissible vibration level according to NO 20-A500-3 for equipment group C is 10 mm/s.

The vibration velocity levels in the area of the portside propeller, outside the extreme ranges - that is, within the engine speed range of 800 to 1,800 rpm are close to the limit of 10 mm/s specified in NO 20-A500-3, but do not exceed it. The same applies to the limit value according to ISO 20816-1, which for Group III, Class C (still acceptable condition) is 11.2 mm/s. Prolonged operation of the propeller in extreme ranges is not recommended. Mandatory, yet abbreviated, propeller tests must include vibration measurements in the Z (H) direction of the accelerometer at speeds above 1,400 rpm.

Single, high-amplitude pulses visible on the portside propeller at low engine speeds (600 rpm) (see Fig. 6), comparable to the vibration amplitude at maximum speed (1900 rpm) of the engine, result from the presence of backlash in the propeller under test. These pulses decrease with increasing load from 600 to 1000–1200 rpm of the engine, and these are the speeds at which the propeller blades reach their maximum deflection.

5.6. Analysis of vibration velocity signals – starboard propeller

The results of the analyses of vibration velocity distributions for individual loads on the starboard propeller are presented in Table 7. The results for all load regimes are shown in Figure 15 for the X (L), Y (H), and Z (V) directions, and for the resultant direction in Figure 16. Table 7 provides a reference to the values specified in ISO 20816-1.

On the starboard propeller of the vessel, unlike the port propeller, there are no visible numerous impulse disturbances indicating play in the mechanical system. For the initial, lowest propeller load of 600 rpm of the engine, corresponding to 32 rpm of the propeller, the permissible V_{RMS} values are exceeded. A similar situation occurs at the maximum propeller load, i.e., at an engine speed of 1900 rpm (99 rpm for the propeller).

The measured vibration velocity values in the X (L) and Y (H) directions are similar across all analysis ranges, with a variation of up to ±10%. The variation in Z (V) values at an engine speed of 1400 rpm also falls within this range, but increases for the last three load ranges, reaching 19%, and at 1800 rpm, even approximately 37%. It should be noted that above 1500 rpm of the engine, and thus 80 rpm of the propeller at 100% propeller blade deflection, the propeller's vibrations are primarily influenced by vibrations in the Z (H) direction. Therefore, this direction of vibration measurement has the most significant impact on the assessment of the ship's propeller vibration level.

The vibration velocity levels in the area of the starboard propeller in the low-frequency range in the Z (V) direction, at the propeller's minimum load at 32 rpm, are nearly 23 mm/s, which, according to NO 20-A500-3, significantly exceeds the permissible limit. Similarly, vibration velocity levels in the area of the starboard propeller in the low-frequency range in the Z (V) direction at the propeller's maximum load 99 rpm are 15.4 mm/s; for the remaining directions, they are lower (in the X (L)

– 13.3 m/s, in the Y (H) direction – 12.9 m/s), but still at a level exceeding the permissible values described in NO 20-A500-3.

Table 7. Effective vibration velocity values for the entire load range of the starboard propeller.

Engine speed – operating mode	Propeller speed – operating mode	RMS vibration velocity V_{RMS} [mm/s] Direction X (L)	Direction Y (H)	Direction Z (V)	*Direction W**	Vibration intensity zone according to ISO 20816-1 for class III
600	32	20,9	20,8	23,0	37,4	D
800	42	8,6	8,7	9,5	15,5	C
1000	53	6,6	6,6	7,3	11,8	C
1200	64	5,7	5,6	6,2	10,1	C
1400	75	5,5	5,5	6,1	9,9	C
1600	91	6,7	6,1	7,2	11,6	C
1800	96	7,4	7,3	10,0	14,4	C
1900	99	13,3	12,9	15,4	24,1	D

** resultant direction.*

The permissible vibration level according to NO 20-A500-3 for equipment group C is 10 mm/s.

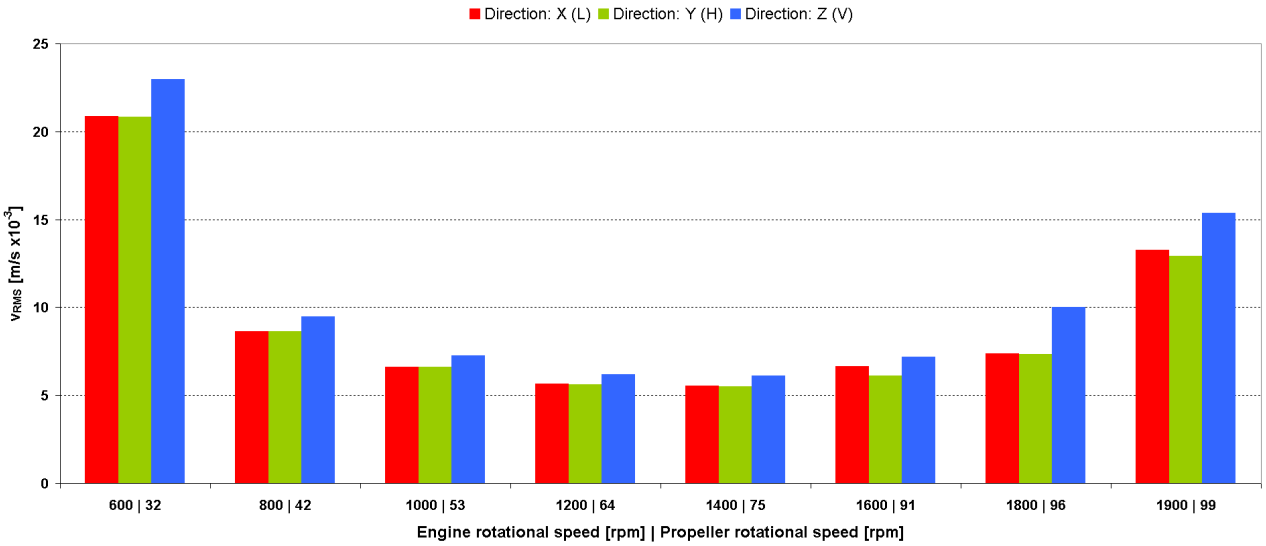

Figure 15. Summary of the root-mean-square values of the starboard propeller's vibration velocity for the entire range of propeller loads as a function of the drive motor's rotational speed in the mutually perpendicular directions X (L), Y (H), and Z (V).

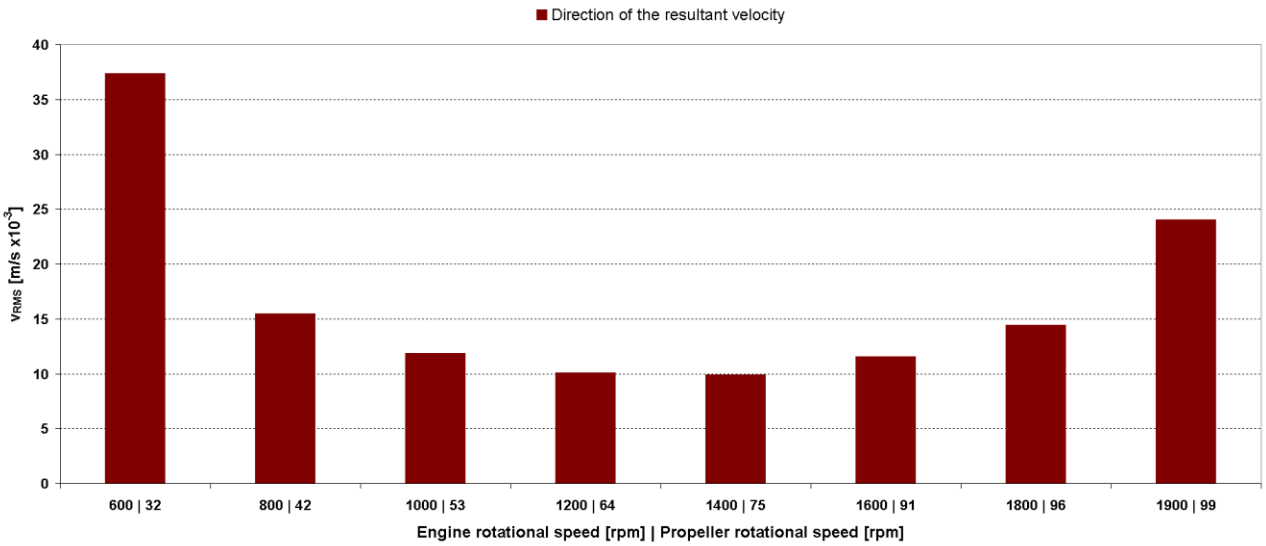

Figure 16. Summary of the root-mean-square vibration velocities in the resultant direction for the starboard propeller across the entire range of propeller loads as a function of the drive motor's rotational speed.

6. Discussion of the research results

Vibroacoustic tests conducted on two Voith Schneider Propeller 21GH/160 propellers revealed a clear asymmetry in the dynamic response of the port and starboard propulsion systems across the entire operating range under test. A comparison of the root-mean-square vibration accelerations shows a difference of over 50% in the worst-case scenario (0.35 m/s² for the port propeller and 0.23 m/s² for the starboard propeller).

The results confirm that the change in vibration levels with increasing load is not monotonic. Elevated values were recorded both at the lowest and highest loads, while a marked increase in vibrations was observed once the propeller exceeded 75 rpm. This range corresponds to the maximum blade deflection and the conditions under which vibrations were felt on the upper decks of the vessel, which further confirms their operational significance.

For the portside propeller, the V_{RMS} values covered by these standards in the X (L), Y (H), and Z (V) directions for analysis intervals 2 through 7 remained below the 10 mm/s limit adopted for Group C equipment in accordance with standard NO-20-A500-3. The vibrations closest to the threshold value were those in the Z (V) axis direction - 9.9 mm/s at a motor speed of 1800 rpm. Based on the measurements in this range, it can be concluded that the left propeller remains in a technically acceptable condition but is operating near the limit of the acceptable vibration level. Under extreme load conditions (analyzed intervals numbered 1 and 8), the vibration velocity values exceed the permissible limit. At the same time, it should be noted that the exceedances concern the calculated root-mean-square values of vibration velocity in the resultant direction, while the directional values remain within acceptable limits, indicating that the assessment of the technical condition should not be based solely on the analysis of vibrations in the direction of individual axes.

A key feature of the portside response was the impulsive nature of the signal at low rotational speeds. The recorded high-amplitude impulse disturbances in the vibration acceleration waveforms, as well as operational observations indicating the presence of play, suggest the possibility of mechanical play, momentary impact contacts, or unstable operation of the bearing components or the blade pitch mechanism. This phenomenon is diagnostically significant, as it may constitute an early symptom of progressive system degradation.

For the starboard propeller, the V_{RMS} values to which the relevant standards refer, in the X (L), Y (H), and Z (V) directions for analysis intervals from 2 to 7, also remained within the 10 mm/s limit adopted for Group C equipment according to NO-20-A500-3. The threshold value was reached in the Z (V) direction at a motor speed of 1800 rpm, as was the case for the port side. Disregarding the results of the right propeller's operation under extreme load conditions, it can be concluded that it remains in a technically acceptable state but operates close to the limit of the acceptable vibration level. Under extreme load conditions, the vibration velocity values exceed the permissible limit.

A clear exceedance of the permissible level by both propellers under both minimum and maximum load conditions indicates a condition requiring diagnostic measures and restrictions on long-term operation.

In both propellers, the vertical Z (V) direction was of the greatest diagnostic significance, indicating that the primary path of dynamic load transmission follows a vertical trajectory. At the same time, the results indicate that the most favorable operating range in terms of vibration intensity is the middle range, approximately 64–75 propeller rpm. The lowest V_{RMS} values were recorded in this range, which is directly relevant for the preliminary determination of a safer operating range.

From a mechanical standpoint, the obtained results should be interpreted as the effect of the coupling of mechanical and hydrodynamic phenomena typical of cycloidal propellers. At low loads, the effects of clearances, momentary contacts, or degraded bearing performance likely dominate, whereas at high loads, the contribution of hydrodynamic forces associated with full blade deflection and increased forces acting in the system increases. This is consistent with literature reports indicating that the dynamic response of VSP propellers results from the strong coupling of hydrodynamics with the structural properties of the blades and the pitch mechanism components. Consequently, the most likely areas of potential failure are: the rotor and blade bearings, the blade pitch mechanism, torque transmission components, and structural connections between the propeller and the hull.

In addition to the scope of analysis required by the

aforementioned ISO 20816 and NO-20-A500 standards, the study also sought to determine changes in commonly known statistical and diagnostic metrics resulting from changes in the operating regime of the power unit. In each of the analyzed intervals, a total of several parameters were determined, of which the most well-known and useful ones are presented in the graphs. The criterion for usefulness was the range of variation of the measures within the analyzed test range. The comparative graphs were prepared on the assumption that a value of 0 on the graph corresponds to the minimum value of the parameter, while 100% corresponds to the maximum value obtained from the analyses for a given propulsion unit. This approach facilitates the determination of a given measure's sensitivity to changes in the operational parameters of the vessel under study. The determination of these measures alone may, in further studies, allow for the detection of signs of wear or emerging malfunctions.

The presented study has high practical value because it was conducted under actual operating conditions, across the full load range, and using triaxial measurements at the same diagnostic point on both propellers. At the same time, their methodological limitations should be noted. The assessment was based primarily on the analysis of time waveforms and V_{RMS} values, without a full spectral analysis, order analysis, or localization of vibration sources at a larger number of measurement points. For this reason, the results reliably identify operating ranges with increased risk and demonstrate the asymmetry in the condition of both propellers, but do not yet allow for the unambiguous attribution of the observed response to a single damaged component. In the next stage of the research, it is planned to expand the scope of measurements to include additional measurement points and an inspection of the bearing mechanism and blade pitch system, to perform modal analysis, and, in the signal processing stage, to include time-frequency and order analyses.

7. Conclusion

The tests confirmed that the dynamic state of both propellers depends on the operating regime in a nonlinear manner. The most unfavorable conditions occurred at 32 and 99 rpm, while a marked increase in vibration levels was observed above 75 rpm.

The propellers under test remain in a technically acceptable state within the tested ranges, but they operate close to the limit of acceptability.

The Z (V) direction proved to be the most sensitive direction for evaluation, and it appears that in operational practice it should be treated as a priority during accelerated testing and trend monitoring.

The most favorable operating range in terms of vibration levels is approximately 64÷75 rpm of the propeller. Extreme load ranges should be kept to a minimum until maintenance is performed. The most likely causes of the observed phenomena are mechanical play, bearing degradation, malfunctions in the blade pitch mechanism, and increased hydrodynamic loads when the blades are fully pitched. To definitively identify the damaged component, the investigation must be expanded to include spectral analysis, time-series analysis, and multipoint measurements.

Vibration spectra in the 0÷500 Hz range serve as a useful diagnostic tool for the propulsion systems under study. They enable the identification of dominant rotational orders, the assessment of vibration energy distribution, the comparison of the dynamic response of the propellers on both sides, and the identification of frequencies that are particularly significant for further diagnosis. In particular, the clear presence of a component corresponding to the fourth harmonic of the motor's rotational speed indicates that this is a fundamental characteristic of the dynamic state under investigation and may serve as a key interpretive parameter in the analysis of VSP rotator operation. It should be emphasized, however, that frequency spectra alone do not yet allow for the unambiguous identification of a specific fault. They can, however, serve as a basis for further analyses, such as row analysis, multi-state comparison, amplitude trend analysis, or correlation with the system's operational parameters. They do, however, serve as a signal for the operator to perform an interim inspection.

References

1. Jürgens D, Palm M, Singer S, Urban K. Numerical optimization of the Voith-Schneiderfi Propeller. ZAMM - Journal of Applied Mathematics and Mechanics / Zeitschrift für Angewandte Mathematik und Mechanik 2007; 87(10): 698–710.

doi:10.1002/zamm.200510345.
2. Voith. Voith Schneider Propeller (VSP). Available from: https://www.voith.com/corp-en/drives-transmissions/ voith-schneider-propeller-vsp.html.
3. Prabhu J J, Dash A K, Nagarajan V, Sunny M R. Vibration analysis of cycloidal propeller blade during ship maneuvering. Journal of Marine Science and Technology 2022; 28(1): 44–71. doi:10.1007/s00773022-00899-1.
4. Halder A, Walther C, Benedict M. Hydrodynamic modeling and experimental validation of a cycloidal propeller. Ocean Engineering 2018; 154: 94–105. doi:10.1016/j.oceaneng.2017.12.069.
5. Halder A, Heimerl J, Benedict M. Hydrodynamic modeling and experimental validation of cycloidal propeller in translational motion. Ocean Engineering 2024; 295: 116826-6. doi:10.1016/j.oceaneng.2024.116826.
6. Tian X, Lou P, Li T, Zhu X. Stern Vibration Response Prediction of a Straight-Bladed Ship. Open Journal of Acoustics and Vibration 2020; (2): 39–48. doi:10.12677/ojav.2020.82006.
7. Jürgens D, Heinke HJ. Voith Schneider Propeller (VSP) - Investigations of the Cavitation Behaviour. MARINTEK (Norwegian Marine Technology Research Institute); 2009.
8. Liu W, Liu Z, Xue W, Chen Q. Unsteady Hydrodynamic Analysis and Experimental Methodology for Voith Schneider Propeller. Journal of Marine Science and Engineering 2025; 13(10): 1933–3. doi:10.3390/jmse13101933.
9. Prabhu J J, Nagarajan V, Sunny M R, Sha O P. On the fluid structure interaction of a marine cycloidal propeller. Applied Ocean Research 2017; 64: 105–127. doi:10.1016/j.apor.2017.01.019.
10. Pyrchla K, Lapiński K, Szulwic J, Jurczak W, Przyborski M, Pyrchla J. Accuracy of marine gravimetric measurements in terms of geodetic coordinates of land reference benchmark. Eksploatacja i Niezawodność – Maintenance and Reliability 2024; 26(3). doi:10.17531/ein/188592.
11. Markuszewski D, Wądołowski M, Krajewski A. The Influence of Variable Stiffness of the Shape Memory Alloys Carbon Composite Structure on Mechanical Vibration. Materials 2024; 17(2): 480–0. doi:10.3390/ma17020480.
12. Kluczyk M, Grządziela A, Batur T. Design and Operational Diagnostics of Marine Propellers Made of Polymer Materials. Polish Maritime Research 2022; 29(4): 115–122. doi:10.2478/pomr-2022-0049.
13. Gorzym M, Markuszewski D. Laboratory Tests of Rolling Resistance of Different Tread Profiles for the Wheel of Martian Roverr. Advances in Science and Technology Research Journal 2024; 18(3): 280–295. doi:10.12913/22998624/186931.
14. Peruń G. Modelowanie dynamiczne układu napędowego z przekładnią obiegową w komputerowym wspomaganiu projektowania i diagnozowania. Monograph. vol. 650. Wydawnictwo Politechniki Śląskiej, Gliwice; 2017.
15. Rosenloecher T, Schlecht B. Kinematics and Load Conditions at a Cycloidal Propeller. The 9th Conference on Computational Methods in Marine Engineering (Marine 2021) 2022; 1(1). doi:10.2218/marine2021.6830.
16. Palm M, Jürgens D, Bendl D. Numerical and Experimental Study on Ventilation for Azimuth Thrusters and Cycloidal Propellers. Proceedings of the Second International Symposium on Marine Propulsors - smp'11, June 2011, Hamburg, Germany. 2022.
17. Klekot G, Dąbrowski Z, Dziurdź J. 50 Years of scientific thought on Machine Diagnostics in Poland and its influence on maritime applications. Polish Maritime Research 2024; 31(4): 161–173. doi:10.2478/pomr-2024-0060.
18. Korczewski Z. A Method to Assess Transverse Vibration Energy of Ship Propeller Shaft for Diagnostic Purposes. Polish Maritime Research 2017; 24(4): 102–107. doi:10.1515/pomr-2017-0141.
19. Liu W, Liu Z, Chen Q, Ma C. Research on Efficiency Optimization of the Voith-Schneider Propeller Based on Motion Curve Parameter Control. Ocean Engineering 2024; 299. doi:10.1016/j.oceaneng.2024.117136.
20. Mohsen K K, Bargash R A. Isolation of Vibration Induced in Drive Type Voith Schneider Propeller due to Rotation of Cycloidal Drive. International Journal of Engineering and Technology 2018; 7(4): 864–869. doi:10.14419/ijet.v7i4.19.28059.
21. Ekine A A, Ubulom A I A. Stress concentration analysis at the blade–strut interface of a Voith schneider propeller using static structural sub-modelling. Global Journal of Engineering and Technology Advances 2026; 27(1): 116–27. doi:10.30574/gjeta.2026.27.1.0079.
22. Zhang G, Zhao Y, Li T, Zhu X. Propeller Excitation of Longitudinal Vibration Characteristics of Marine Propulsion Shafting System. Shock and Vibration 2014; 2014: 1–19. doi:10.1155/2014/413592.
23. Batrak Y A, Shestopal V P, Batrak R Y. Propeller hydrodynamic loads in relation to propulsion shaft alignment and vibration calculations.

SNAME 13th Propeller and Shafting Symposium 2012. doi:10.5957/pss-2012-010.

24. Liu Z, Yan H, Shi Z, Xia D. Two-Dimensional Dynamics CFD Simulation of Voith-Schneider Cycloidal Propeller. 2023 IEEE International Conference on Mechatronics and Automation (ICMA) 2023: 1395–1400. doi:10.1109/icma57826.2023.10216048.
25. Standard ISO 20816-1, Mechanical vibration — Measurement and evaluation of machine vibration – Part 1: General guidelines.
26. Standard NO-20-A500-1-3:2017, Technical Requirements and Testing of Ship Equipment and Mechanisms – Vibrations - Measurements and Evaluation Criteria.
27. IMI SENSORS . Model 604B91 Triaxial ring-style, industrial, ceramic shear ICPfi accel, 100 mV/g, 0.5 to 5k Hz, side exit, 4-pin M12 conn., triaxial single point ISO 17025 accredited calibration Installation and Operating Manual. Manual 21354 Rev E ECN 50523.
28. Cempel C. Diagnostyka wibroakustyczna maszyn. Wydawnictwo Politechniki Poznańskiej, Poznań; 1985.
29. Madej H. Diagnozowanie uszkodzeń mechanicznych w silnikach spalinowych maskowanych przez elektroniczne urządzenia sterujące. ITE Katowice-Radom; 2009.
30. Peruń G, Opasiak T. Assessment of technical state of the belt conveyor rollers with use vibroacoustics methods - preliminary studies. Diagnostyka 2016; 17(1): 75–80.
31. Klekot G. Zastosowanie miar propagacji energii wibroakustycznej do monitorowania stanu obiektów oraz jako narzędzie w zarzadzaniu hałasem. ITE, Radom; 2012.
32. Szabatin J. Podstawy teorii sygnałów. Wydawnictwo Komunikacji i Łączności, Warszawa; 2008.
33. Zieliński T. Od teorii do cyfrowego przetwarzania sygnałów. Wydział EAIiE AGH, Kraków; 2002.
34. Dziurdź J. Application of Correlation and Coherence Functions in Diagnostic Systems. Solid State Phenomena 2013; 196: 3–12. doi:10.4028/www.scientific.net/ssp.196.3.
35. Randall R. Frequency Analysis. Bruel Kjaer, Naerum; 1987.
36. Li J, Wu C, Li H. Bearing fault monitoring system of train running gear based on complex morlet wavelet. Instrum Tech Sens. 2022; 7(8): 63–68. doi:10.3969/j.issn.1002-1841.2022.08.012.

Appendix 1. Full time courses of vibration accelerations recorded on the portside propeller of the ship.

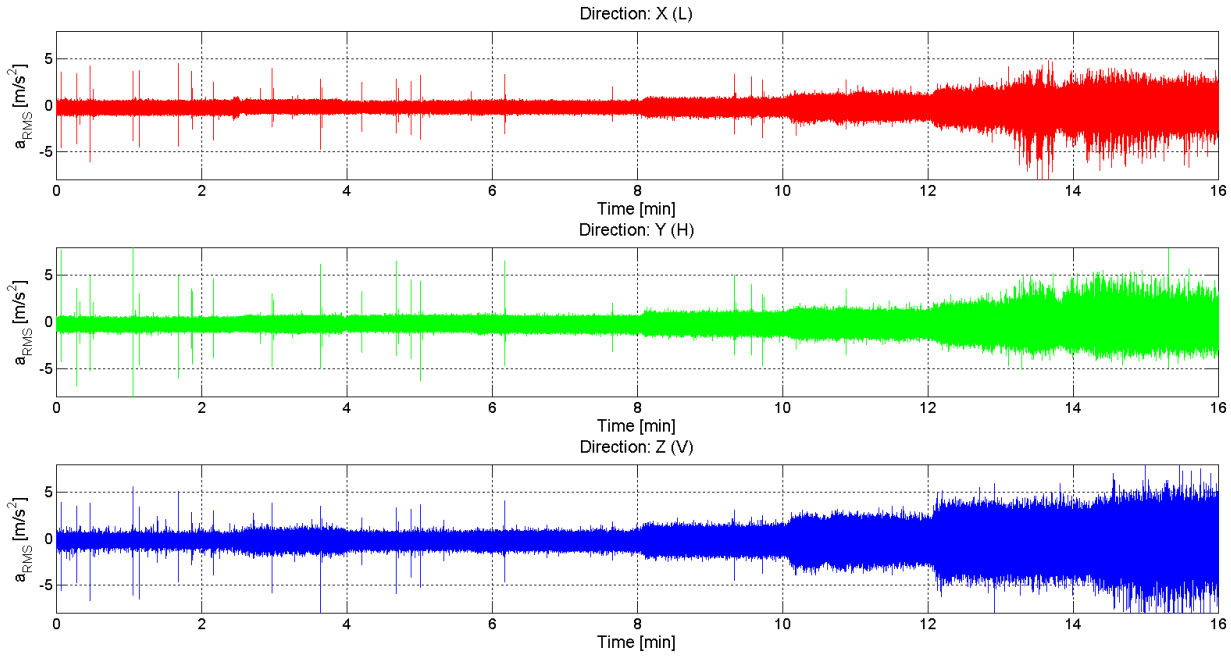

Figure A1. Time courses of vibration accelerations recorded on the ship's port propeller for all mutually perpendicular measurement directions, in the order X (L), Y (H), Z (V).

Appendix 2. Summary of effective vibration accelerations in the resultant direction for the port propeller across the entire range of

propeller loads as a function of the drive motor's rotational speed.

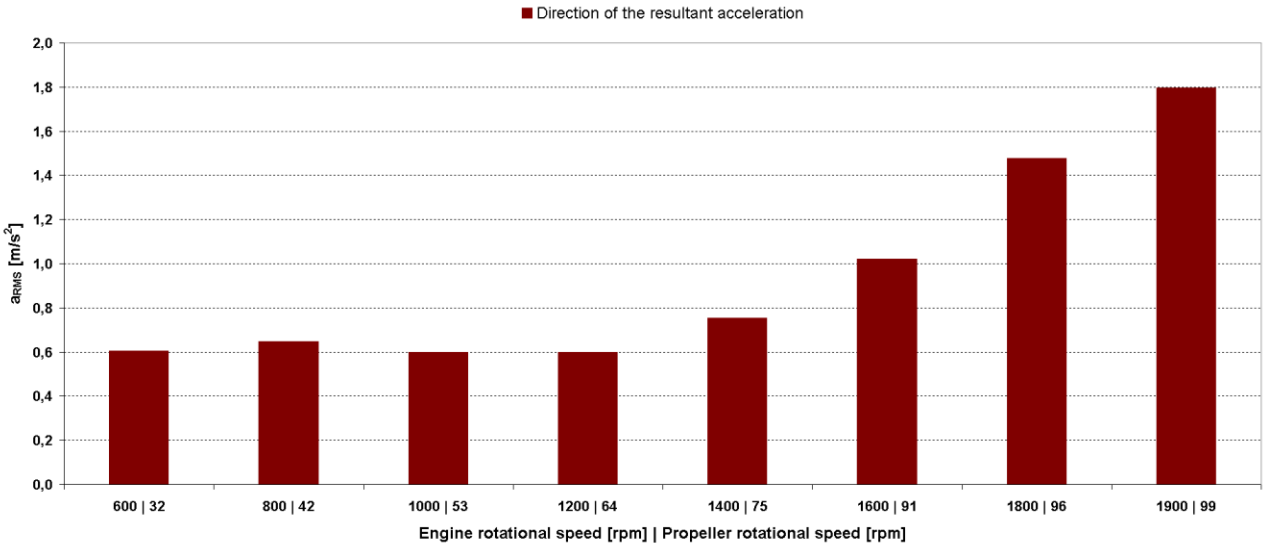

Figure A2. Summary of the root-mean-square vibration accelerations in the resultant direction for the portside propeller across the entire range of propeller loads as a function of the drive motor's rotational speed.

Appendix 3. Full time courses of vibration accelerations recorded on the starboard propeller of the ship.

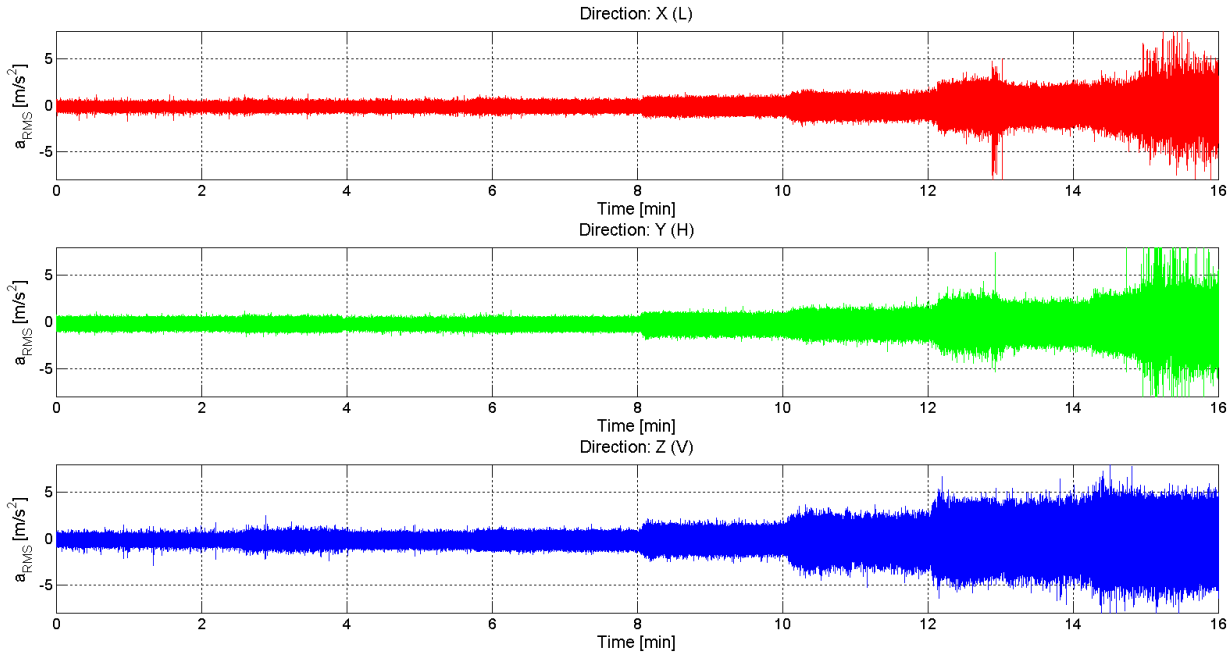

Figure A3. Time courses of vibration accelerations recorded on the ship's starboard propeller for all mutually perpendicular measurement directions, in the order X (L), Y (H), Z (V).

Appendix 4. Summary of effective vibration accelerations in the resultant direction for the starboard propeller across the entire range of propeller loads as a function of the drive motor's rotational speed.

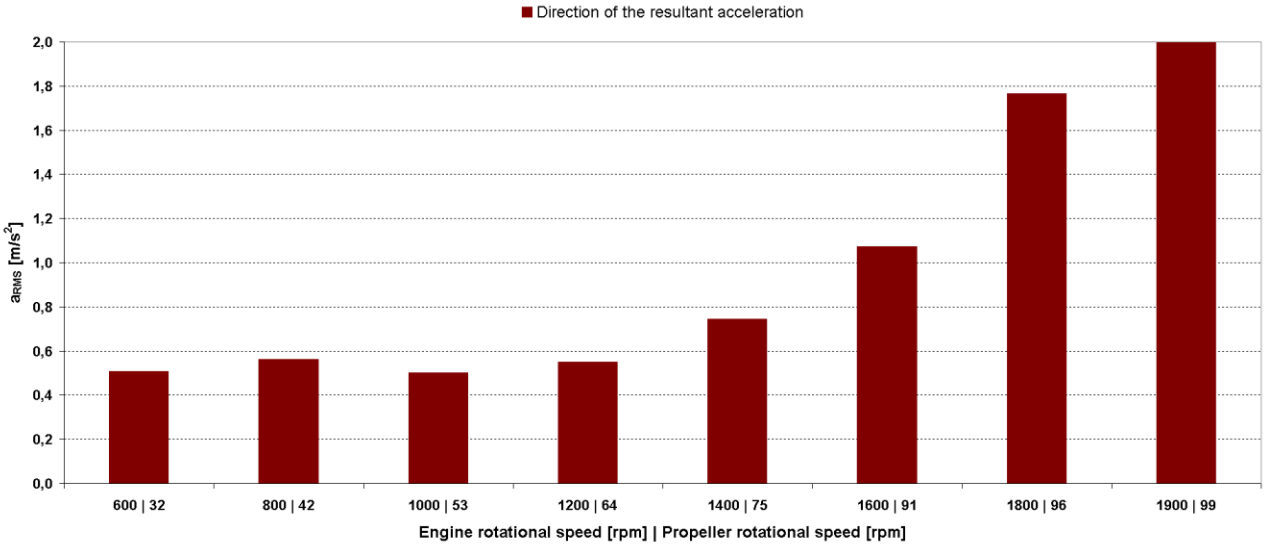

Figure A4. Summary of the root-mean-square vibration accelerations in the resultant direction for the starboard propeller across the entire range of propeller loads as a function of the drive motor's rotational speed.